Chapter 4

Influence of Structural Changes on Electronic Properties of *ansa*-Metallocenes of Groups 5-7

4.1 Introduction to Chapter 4

This chapter is again concerned with structure-reactivity relationships in metallocene chemistry. In particular the influence of structural changes on the electronic and bonding properties of the metallocene unit is addressed. The first part of this chapter describes the preparation of a new cationic Group 6 *ansa*-metallocene trihydride (**Section 4.2**). These compounds exhibit large, temperature dependent H-H coupling constants in the ^{1}H NMR spectra. The synthesis and molecular structure of the first carbon-bridged *ansa*-rhenocene complex is presented in the second part of this chapter (**Section 4.4**). Density functional calculations of the electronic structure of this new compound are used to explain unexpected features of the molecular structure.

4.2 Quantum Mechanical Exchange Coupling in *ansa*-Tungstenocene Trihydride Cations

4.2.1 Introduction

As outlined in **Section 1.5.4**, the H_A-H_B coupling constant J_{AB} has been shown to vary by several orders of magnitude when an *ansa*-bridge is introduced between the cyclopentadienyl rings of the *bis(*cyclopentadienyl)tungsten trihydride cation. $[W(\eta\text{–}C_5H_5)_2H_3][Cl]$ shows a normal J_{AB} value of 8.5 Hz at all temperatures.[1] When an *ansa*-bridge is introduced the values are significantly different. For $[W\{(\eta\text{–}C_5H_4)SiMe_2(\eta\text{–}C_5H_4)\}H_3][BF_4]$ J_{AB} varies from 8 Hz at 133 K to 75 Hz at 273 K, while for the analogous ethylene-bridged species $[W\{(\eta\text{–}C_5H_4)C_2Me_4(\eta\text{–}C_5H_4)\}H_3][Cl]$ J_{AB} is found to vary from 8 Hz at 193 K to 35 Hz at 263 K.[2] However the single carbon-bridged species $[W\{(\eta\text{–}C_5H_4)CMe_2(\eta\text{–}C_5H_4)\}H_3][PF_6]$ shows more extreme behaviour with J_{AB} varying from 2900 Hz at 133 K to 16000 Hz at 203 K.[3] The principal change in this series is that the inter-ring angle α increases (i.e. the bending angle β decreases) as the bridge becomes more sterically constraining.

Prior to this work a number of transition metal polyhydride systems had been identified for which the ^{1}H NMR spectra of an AB_x system show large temperature dependent coupling constants.[4] Such complexes include the *bis(*cyclopentadienyl) metal trihydride species $[M(\eta\text{–}C_5H_{5-x}R_x)_2H_3]^{n+}$ (M = Nb, Ta, n = 0 R = H, $SiMe_3$; M = Mo,

n = 1, R = H),[5-7] the dihydride systems $[M(\eta-C_5H_5)_2H_2(L)]$ (M = Nb, Ta, L = PR_3, CO, CNR)[8-10] and the cyclopentadienyl metal trihydride phosphine systems $[M(\eta-C_5H_5)(L)H_3]$ (M = Rh, Ir; L = PMe_3, $AsMe_3$).[7, 11-13] Values of J_{AB} between 30 and 1500 Hz have been reported for such species.

This phenomenon has been explained in terms of the ability of the hydride ligands to undergo quantum mechanical exchange coupling.[13] There are two distinct contributions to the observed coupling $J_{AB,}$ where J_{AB} is given by the equation:

$$J_{AB} = -2J_{ex} + J_m$$

J_m, the classical component, is the result of conventional Fermi contact interaction and is independent of temperature. J_m typically takes on a value between 2 and 28 Hz. The second component J_{ex} represents the quantum mechanical exchange coupling between two adjacent hydrides in the metal hydride system. This coupling arises from the quantum mechanical exchange of a pair of identical hydrogens, H_1 and H_2, between two chemically inequivalent sites, A and B.

Two equivalent configurations i.e. H_1 and H_2 at sites A and B respectively or H_2 and H_1 at sites A and B respectively, can be associated with two potential energy wells separated by an energy barrier (a "double-well" model) as depicted in **Figure 4.1**.[12] If the barrier between the wells is infinite two uncoupled stationary states ψ_1 and ψ_2 are located in each side of the double well with energies $E_1 = E_2$. However when the barrier is finite two new stationary states $\psi_{1'}$ and $\psi_{2'}$ have associated energies E_+ and E_-. Thus an energy splitting appears according to the equation:

$$E_+ - E_- = -2J_{ex}$$

J_{ex} is intrinsically negative and thus gives rise to a positive contribution to the observed coupling constant J_{AB}.

The current understanding of the phenomenon has been well summarised in recent reviews by Sabo-Etienne and Chaudret and Eisenstein *et al*. and is outlined below:[4]

(i) A soft MH_2 bending vibration (a "wagging" motion) allows close approach of the two exchanging hydrogens. In the case of a $MH_A(H_B)_2$ system this bending vibration involves the central (H_A) and one of the lateral (H_B) hydrogens.

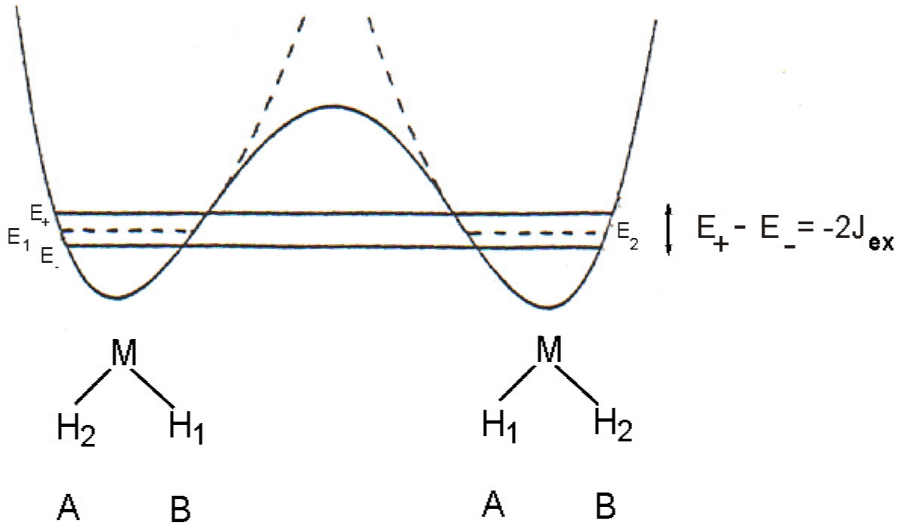

Figure 4.1 The double well model for quantum mechanical exchange of equivalent hydrogens H_1 and H_2 between two inequivalent sites A and B.

(ii) This vibration initiates a chemical pathway to exchange which brings the exchanging hydrogens to an approach which is shorter than the sum of their van der Waals radii. A coordinated dihydrogen complex may exist as a minimum along this pathway.

(iii) The barrier to chemical (classical) exchange must be between 35 and 70 $kJmol^{-1}$ to allow quantum mechanical exchange coupling to be observable by ^1H NMR spectroscopy. If the barrier is too high the quantum mechanical exchange coupling is too small to be observed, whereas if the barrier is too small classical exchange leads to signal coalescence.

(iv) There is rotational and vibrational tunnelling through the energy barrier between the two potential energy wells.

(v) The observed temperature dependence of J_{ex} is a consequence of thermal population of excited vibrational states.

In the light of the remarkable coupling constant observed for $[W\{(\eta\text{–}C_5H_4)CMe_2(\eta\text{–}C_5H_4)\}H_3][PF_6]$ it was decided to further explore the nature of quantum mechanical exchange coupling. The primary aim of this work was to investigate whether such large coupling constants are general for highly strained *ansa*-metallocene trihydrides.

4.2.2 Preparation of [W{(η–C_5H_4)C(C_5H_{10})(η–C_5H_4)}Cl_2] (34)

The cyclohexyl-bridged molybdenum compound [Mo{(η–C_5H_4)C(C_5H_{10})(η–C_5H_4)}Cl_2] has been prepared previously in this laboratory *via* the reaction between $MoCl_4$.DME and [Li_2{(C_5H_4)C(C_5H_{10})(C_5H_4)}] in diethyl ether.[3] No further chemistry of this system was explored.

The compound [W{(η–C_5H_4)C(C_5H_{10})(η–C_5H_4)}Cl_2] **(34)** was prepared *via* an analogous procedure by the reaction between WCl_4.DME and [Li_2{(C_5H_4)C(C_5H_{10})(C_5H_4)}] (**Scheme 4.1**). Extraction of the reaction mixture into dichloromethane afforded the compound **34** as a pale brown solid in 28 % yield.

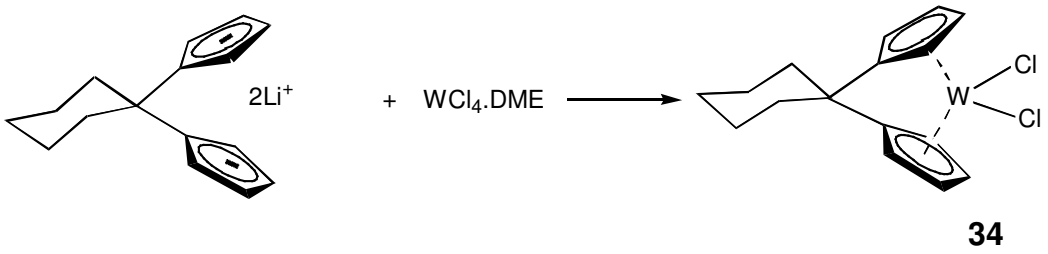

34

Scheme 4.1 Preparation of [W{(η–C_5H_4)C(C_5H_{10})(η–C_5H_4)}Cl_2] **(34)**

The compound **34** was characterised by ^1H and $^{13}C\{^1H\}$ NMR spectroscopy and FAB mass spectrometry. Elemental analyses were consistent with the proposed empirical formula. The FAB mass spectrum of the compound **34** shows a peak due to the molecular ion and a peak due to the fragment ion resulting from the loss of one Cl ligand.

The ^1H NMR spectrum of the compound **34** consists of two partial triplets at δ 5.95 and 5.45 ppm corresponding to the protons of the cyclopentadienyl rings. Two multiplet resonances at δ 1.46 and 1.12 ppm are assigned to six and four protons of the cyclohexyl bridge respectively. The $^{13}C\{^1H\}$ NMR spectrum is more informative with regard to the conformation of the bridging unit. The bridgehead carbon is located as a weak resonance at δ 34.7 ppm. The three inequivalent carbons of the cyclohexyl bridge are assigned to resonances at δ 31.2, 25.7 and 20.9 ppm.

4.2.3 Preparation of [W{(η–C_5H_4)C(C_5H_{10})(η–C_5H_4)}Me_2] (35)

Dimethyl derivatives of Group 6 *ansa*-metallocenes have proved to be particularly conducive to the growth of single crystals suitable for X-ray molecular structure determination.[2, 3] The compound [W{(η–C_5H_4)C(C_5H_{10})(η–C_5H_4)}Me_2] **(35)** was prepared principally as a means of obtaining the first structurally characterised cyclohexyl-bridged mononuclear *ansa*-metallocene of the general formula [M{(η–C_5H_4)C(C_5H_{10})(η–C_5H_4)}X_2]. The compound [W{(η–C_5H_4)C(C_5H_{10})(η–C_5H_4)}Me_2] **(35)** was prepared by the action of $ZnMe_2$ on a suspension of the compound **34** in toluene at low temperature (**Scheme 4.2**). Following removal of excess $ZnMe_2$ the compound **35** was recrystallised from a concentrated pentane solution at -80 ºC and obtained as an orange crystalline solid in 31 % yield.

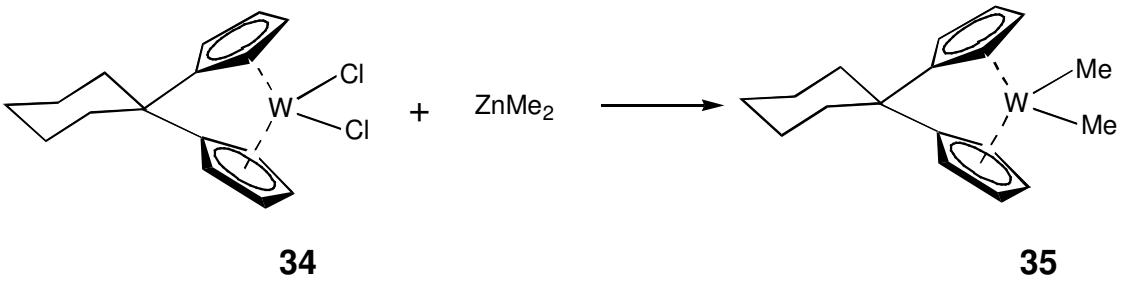

34 **35**

Scheme 4.2 Preparation of [W{(η–C_5H_4)C(C_5H_{10})(η–C_5H_4)}Me_2] **(35)**

The compound **35** was characterised by elemental analysis, FAB mass spectrometry and ^1H and $^{13}C\{^1H\}$ NMR spectroscopy. The FAB mass spectrum of the compound **35** shows peaks due to the molecular ion and fragmentation products arising from the sequential loss of the methyl ligands. The ^1H and $^{13}C\{^1H\}$ NMR spectra of the compound **35** are straightforward and not discussed further here.

Slow cooling of a concentrated solution of the compound **35** in pentane to -80 °C afforded single crystals suitable for X-ray molecular structure determination. The crystal structure was determined and the molecular structure is shown in **Figure 4.2**. Selected interatomic distances and angles and other structural information are presented in **Table 4.1**. Full details of the molecular structure determination are given in **Appendix F**. The compound crystallises in the triclinic space group PI.

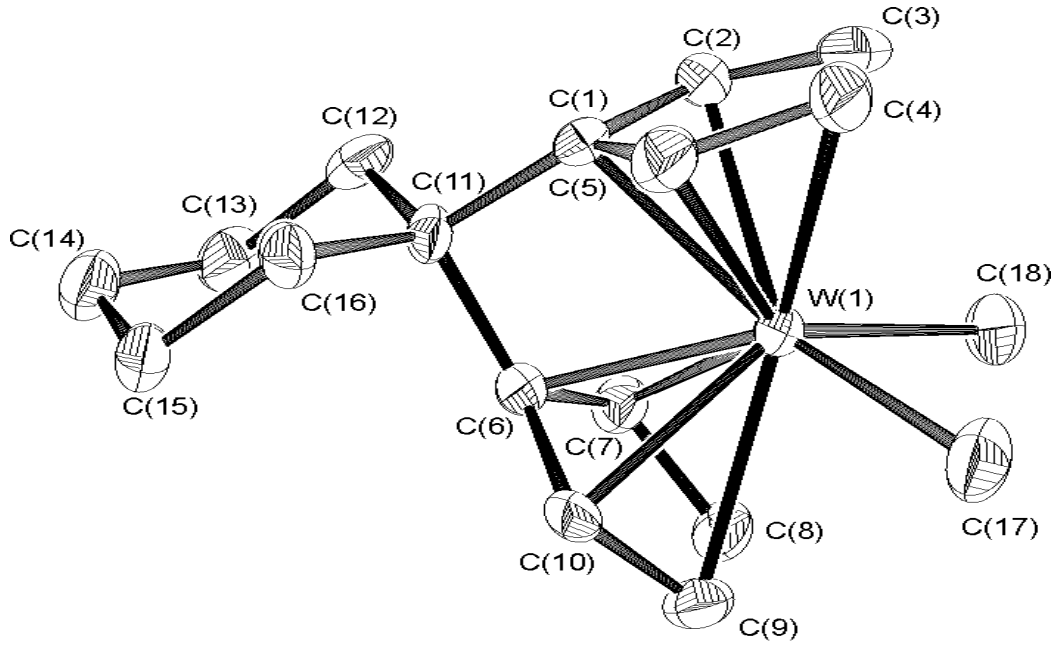

Figure 4.2 Molecular structure of $[W\{(\eta-C_5H_4)C(C_5H_{10})(\eta-C_5H_4)\}Me_2]$ **(35).** Hydrogen atoms are omitted for clarity.

	Length / Å		Angle / °
W-Cp^1_{cent}	1.938	Between Cp planes, α	61.7
W-Cp^1_{ave}	2.323(7)	Cp^1_{norm}-W-Cp^2_{norm}, β	118.3
W-Cp^2_{cent}	1.932	Cp^1_{cent}-W-Cp^2_{cent}, χ	127.6
W-Cp^2_{ave}	2.278(6)	C_{ipso}-Cp plane, ϕ	24.1, 25.2
W-C(1)	2.3041(13)	C_{ipso}-C(11)-C_{ipso}, ε	95.5(3)
W-C(3)	2.4274(15)	C(17)-W-C(18)	78.1(3)
W-C(17)	2.218(7)		
ΔCp^1	0.0325		

Cp^1 = Ring C(1)-C(5), Cp^2 = Ring C(6)-C(10)

Table 4.1 Selected interatomic distances and angles and other structural information for $[W\{(\eta-C_5H_4)C(C_5H_{10})(\eta-C_5H_4)\}Me_2]$ **(35)**

The geometric constraint imparted by the cyclohexyl bridging unit is evident on inspection of the molecular structure of the compound **35**. As expected the bending angle (β = 118.3°) is similar to that found in the analogous compound [W{(η–C_5H_4)CMe_2(η–C_5H_4)}Me_2] (β = 119.1°)[3] . Thus the cyclohexyl bridge C(C_5H_{10}) can be said to exert a similar influence on the structural geometry of the metallocene as the widely studied CMe_2 unit. The shortest metal-ring distance is found between the metal and the *ipso*-carbon indicating that the *ansa*-bridge is pulling the rings away from the metal and opening up the coordination site on the opposite face. Furthermore the C-C bond furthest from the *ipso*-carbon is found to be the shortest such distance in the cyclopentadienyl ring, as evidenced by a value of ΔCp^1 = 0.0325 Å. (ΔCp = (Average of the four longest ring C-C distances) - (Shortest ring C-C distance)). Such structural features imply a significant contribution to bonding in the ring from an η^3-allyl resonance structure (**Section 2.5.1**).

4.2.4 Preparation of [W{(η–C_5H_4)C(C_5H_{10})(η–C_5H_4)}H_2] (36)

Treatment of the compound **34** with $LiBEt_3H$ in THF at low temperature gives the compound [W{(η–C_5H_4)C(C_5H_{10})(η–C_5H_4)}H_2] **(36)** as a pale yellow solid in 42 % yield in a procedure analogous to that used to prepare the compound [W{(η–C_5H_4)CMe_2(η–C_5H_4)}H_2] (**Scheme 4.3**).[3] The use of the Group 13 metal hydrides $NaBH_4$ or $LiAlH_4$ leads to the formation of the compound **36** in very low yield along with other species containing metal-hydride bonds. Interestingly the reaction of [W{(η–C_5H_4)C_2Me_4(η–C_5H_4)}Cl_2] with $LiAlH_4$ gives [W{(η–C_5H_4)C_2Me_4(η–C_5H_4)}H_2] in good yield.[2]

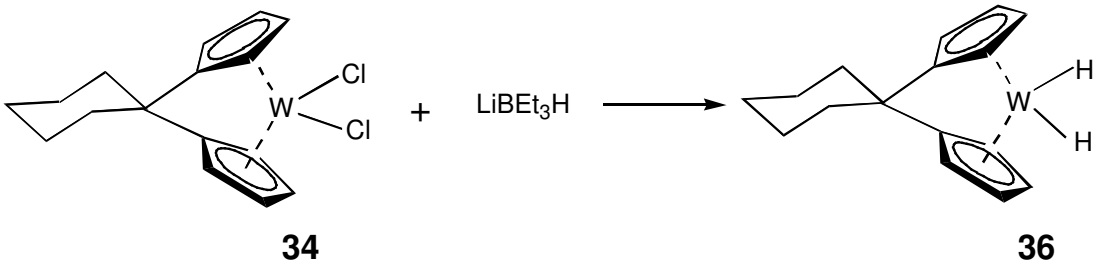

34 **36**

Scheme 4.3 Preparation of [W{(η–C_5H_4)C(C_5H_{10})(η–C_5H_4)}H_2] **(36)**

The compound **36** was characterised by elemental analysis, FAB mass spectrometry, ^{1}H and $^{13}C\{^{1}H\}$ NMR spectroscopy and IR spectroscopy. Of particular note in the ^{1}H NMR spectrum of the compound **36** is a singlet at δ -7.39 ppm assigned to the hydrogens attached to the metal. Such a high field resonance is characteristic of a transition metal hydride species. Associated with this singlet are ^{183}W (I = ½) satellites with $^{1}J_{WH}$ = 94 Hz. $^{1}J_{WH}$ for a number of analogous tungstenocene dihydrides are presented in **Table 4.2**. It is seen that $^{1}J_{WH}$ is significantly increased for the single carbon-bridged species relative to that found for the nonbridged compound $[W(\eta\text{–}C_5H_5)_2H_2]$. The intermediacy of the effect imparted by a silicon- or ethylene-bridge is reflected in values of $^{1}J_{WH}$ = 79 and 80 Hz for the compounds $[W\{(\eta\text{–}C_5H_4)SiMe_2(\eta\text{–}C_5H_4)\}H_2]$ and $[W\{(\eta\text{–}C_5H_4)C_2Me_4(\eta\text{–}C_5H_4)\}H_2]$ respectively.

Compound	$^{1}J_{WH}$/Hz	ν(W-H)/cm^{-1}	Reference
$[W(\eta\text{–}C_5H_5)_2H_2]$	73	1896	1, 14
$[W\{(\eta\text{–}C_5H_4)C_2Me_4(\eta\text{–}C_5H_4)\}H_2]$ **(38)**	80	1875. 1860	2, this work
$[W\{(\eta\text{–}C_5H_4)SiMe_2(\eta\text{–}C_5H_4)\}H_2]$	79	1865	2
$[W\{(\eta\text{–}C_5H_4)SiEt_2(\eta\text{–}C_5H_4)\}H_2]$	79	1881, 1870	2
$[W\{(\eta\text{–}C_5H_4)CMe_2(\eta\text{–}C_5H_4)\}H_2]$	92	1833, 1823	3
$[W\{(\eta\text{–}C_5H_4)C(C_5H_{10})(\eta\text{–}C_5H_4)\}H_2]$ **(36)**	94	1828, 1816	This work

Table 4.2 Comparison of $^{1}J_{WH}$ in the ^{1}H NMR spectrum and selected ν(W-H) in the IR spectrum of tungstenocene dihydride compounds

The IR spectrum of the compound **36** was obtained as a Nujol mull. Two strong bands are seen at 1828 and 1816 cm^{-1} and are attributed to W-H stretching modes. These values are also compared to analogous compounds in **Table 4.2**. It can be seen that in the presence of an *ansa*-bridge ν(W-H) is reduced. This reduction is most marked for the single carbon-bridged compounds **36** and $[W\{(\eta\text{–}C_5H_4)CMe_2(\eta\text{–}C_5H_4)\}H_2]$ suggesting a weakening of the W-H bond. Density functional calculations have shown that as the angle between the rings, α, is increased and thus the corresponding bending angle β decreased, additional ligands at the metal become more weakly bound (**Section 2.6.2-2.6.3**).

4.2.5 Preparation of $[W\{(\eta-C_5H_4)C(C_5H_{10})(\eta-C_5H_4)\}H_3][BF_4]$ (37)

The d^2 dihydride species $[W(\eta-C_5R_5)_2H_2]$ (R = H, Me), in which the lone pair of electrons are located in the central $4a_1$ orbital, are basic and readily protonated by the addition of acid. Direct protonation of the central $4a_1$ orbital has been implied by the deuteration of $[W(\eta-C_5Me_5)_2H_2]$ giving 90 % of the central isotopomer rather than the lateral one (**Figure 4.3**).[15] Protonation of such compounds is reversible and the dihydride species can be obtained quantitatively on treatment with a base such as sodium hydroxide.

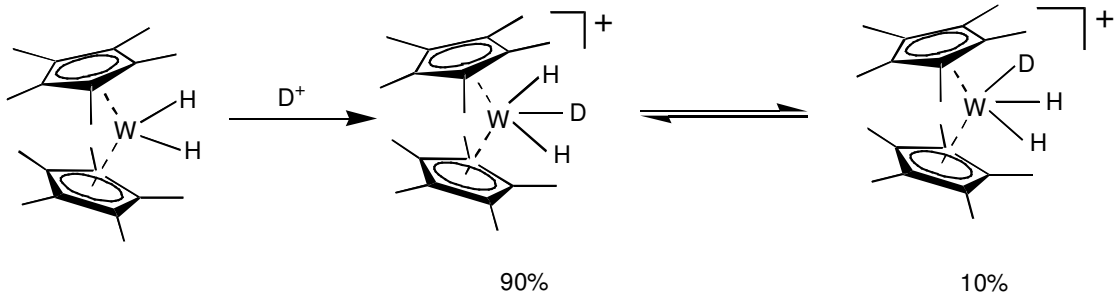

Figure 4.3 Deuteration of $[W(\eta-C_5Me_5)_2H_2]$

The addition of a solution of HBF_4 in diethyl ether to a suspension of the compound **36** in diethyl ether gives the cationic hydride species $[W\{(\eta-C_5H_4)C(C_5H_{10})(\eta-C_5H_4)\}H_3][BF_4]$ **(37)** as a flocculent, air-sensitive white solid in 83 % yield (**Scheme 4.4**)

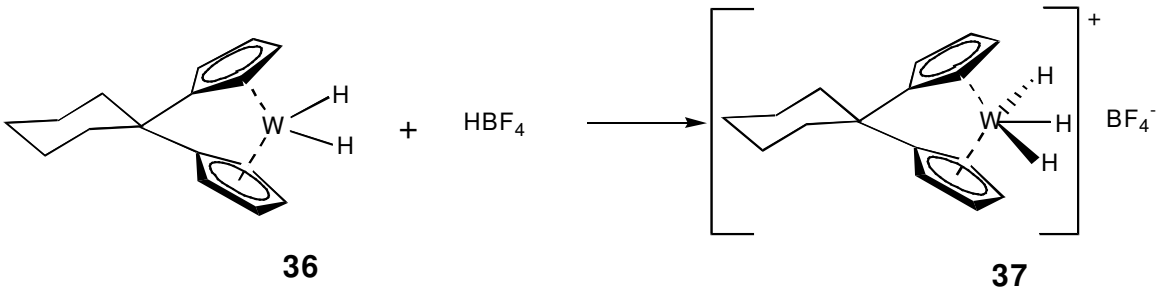

Scheme 4.4 Preparation of $[W\{(\eta-C_5H_4)C(C_5H_{10})(\eta-C_5H_4)\}H_3][BF_4]$ **(37)**

The compound **37** was characterised by ^{1}H, $^{13}C\{^{1}H\}$ and ^{11}B NMR spectroscopy and IR spectroscopy. Elemental analysis was precluded by the extremely air-sensitive nature of the compound. The IR spectrum of the compound **37** shows a strong band at 1898 cm^{-1} corresponding to a W-H stretching mode. The analogous stretch in the nonbridged compound $[W(\eta-C_5H_5)_2H_3][Cl]$ is found at 1932 cm^{-1} and again a reduction in W-H bond strength upon the introduction of a highly constraining bridging unit is indicated.[16]

The ^{1}H NMR spectrum of the compound **37** is of particular interest. In the room temperature spectrum the expected peaks for the $[W\{(\eta-C_5H_4)C(C_5H_{10})(\eta-C_5H_4)\}]$ fragment are observed. The protons of the trihydride unit occur as a broad singlet at δ -3.10 ppm, implying that chemical exchange between the central (H_A) and lateral (H_B) hydrogens is fast on the NMR time scale. The exchange process was investigated further by variable temperature ^{1}H NMR spectroscopy and spectra of the compound **37** in the low melting point solvent $CDFCl_2$ between 147 and 293 K are shown in **Figure 4.4**. The broad resonance at δ -3.10 ppm decoalesces as the chemical exchange process is frozen out and splits into a number of sharp lines below 223 K consistent with a highly second-order AB_2X (A, B = ^{1}H; X = ^{183}W) system.

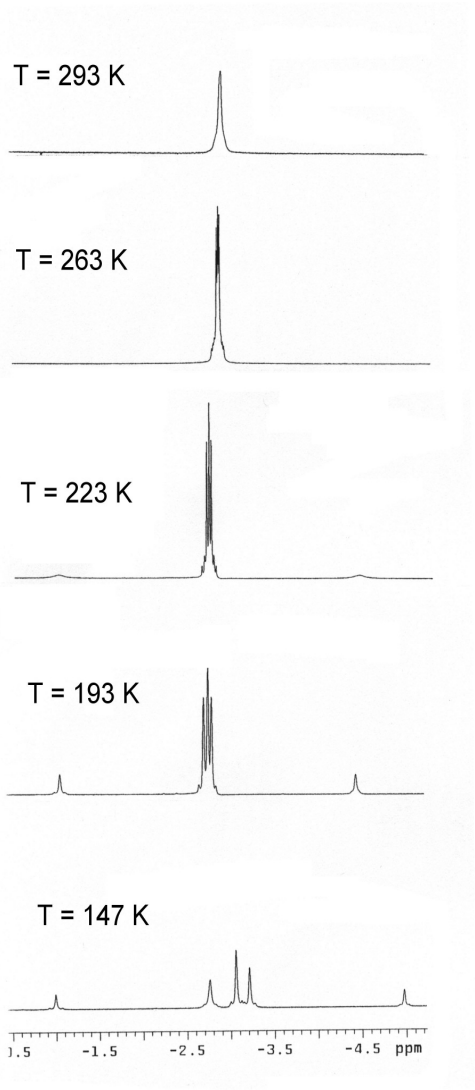

Figure 4.4 High field variable temperature ^{1}H NMR spectra for the compound $[W\{(\eta\text{–}C_5H_4)C(C_5H_{10})(\eta\text{–}C_5H_4)\}H_3][BF_4]$ **(37)** in $CDFCl_2$

Due to the highly second-order nature of the coupling pattern observed for the compound **37** values of δ_A, δ_B and J_{AB} at T = 147 – 223 K could only be determined indirectly by modelling with a spectral spin simulation program. In this case the program *gNMR* was used with full-line shape analysis employed to fit the calculated spectra to the observed spectra.[17] Values obtained for δ_A, δ_B and J_{AB} are presented in **Table 4.3**. R represents a residual factor from the iteration process. Experimental and simulated variable temperature ^{1}H NMR spectra between 163 and 213 K are shown in **Figure 4.5**. In order to successfully simulate the spectra it proved necessary to fix the value of $^{1}J_{WH}$ for both H_A and H_B. $^{1}J_{WH}$ = 60 Hz was chosen as a reasonable value by analogy to $^{1}J_{WH}$ for

other tungstenocene trihydrides. Values of δ_A, δ_B and J_{AB} calculated by the iteration process were found to be insensitive to changes in $^1J_{WH}$.

T/K	δ_A/ppm	δ_B/ppm	J_{AB}/Hz	R/10^{-3}
223	-0.818	-4.071	17500	7.22
213	-0.913	-3.986	14500	1.89
203	-0.986	-4.041	13100	1.01
193	-0.942	-4.014	10400	3.31
183	-1.115	-4.138	7800	1.97
173	-1.084	-4.139	6100	3.45
163	-1.017	-4.041	4200	4.01
147	-0.975	-4.005	2900	1.97

Table 4.3 ^{1}H NMR spectral parameters for the compound $[W\{(\eta\text{–}C_5H_4)C(C_5H_{10})(\eta\text{–}C_5H_4)\}H_3][BF_4]$ **(37)** derived from spin simulation program *gNMR*

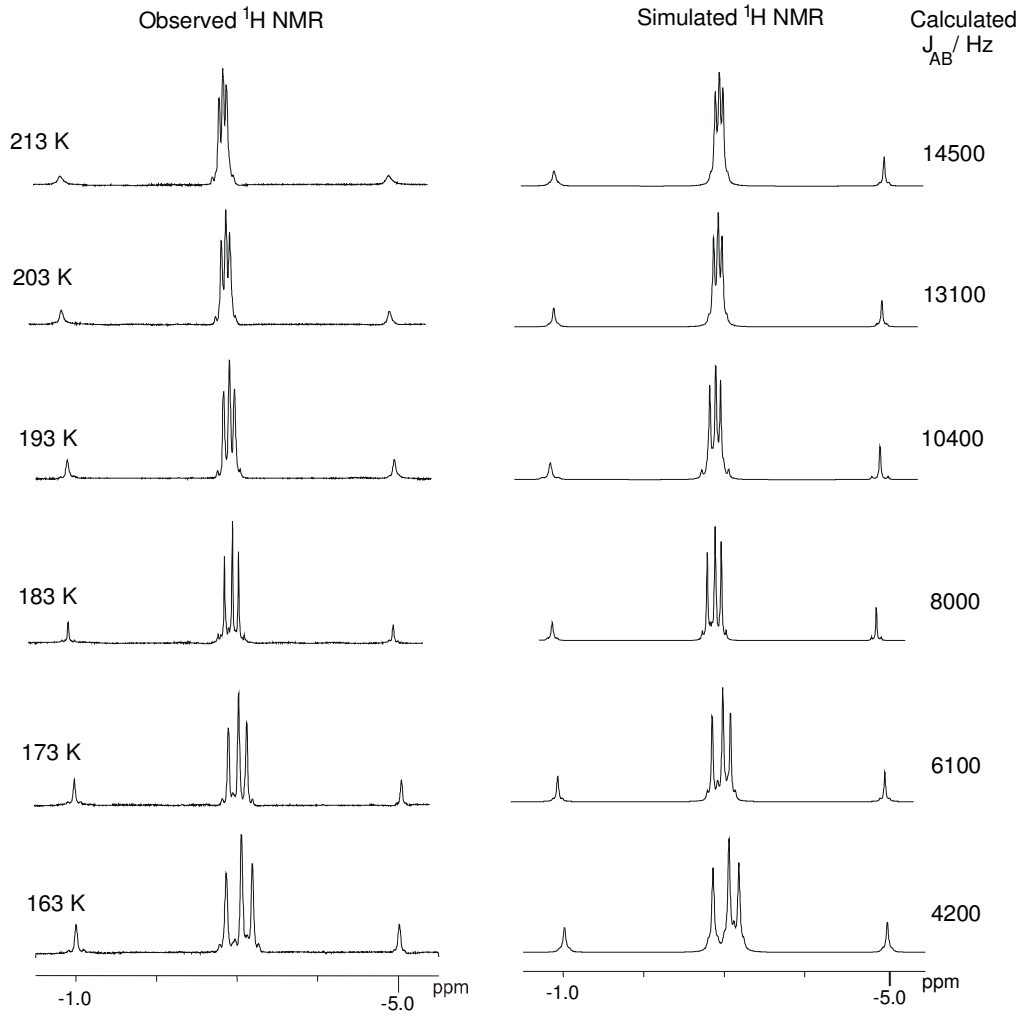

Figure 4.5 Observed and simulated variable temperature ^{1}H NMR spectra for the compound $[W\{(\eta-C_5H_4)C(C_5H_{10})(\eta-C_5H_4)\}H_3][BF_4]$ **(37)**

The H-H coupling constant J_{AB} is found to be highly temperature dependent and extremely large. At 223 K, the highest temperature at which it was possible to calculate J_{AB}, a value of *ca.* 17500 Hz is determined. The magnitude of J_{AB} is similar to that found for the analogous compound $[W\{(\eta-C_5H_4)CMe_2(\eta-C_5H_4)\}H_3][PF_6]$ and is considerably larger than J_{AB} reported for other polyhydride systems. A plot of J_{AB} against temperature is shown in **Figure 4.6** and shows that the rate of increase in J_{AB} increases with temperature. This is consistent with the predicted exponential relationship between J_{ex} and temperature.[7] Clearly J_{AB} is expected to increase further although the onset of chemical exchange prevents the determination of J_{AB} above 223 K. At the lowest accessible temperature (T = 147 K) J_{AB} is calculated to be 2900 Hz.

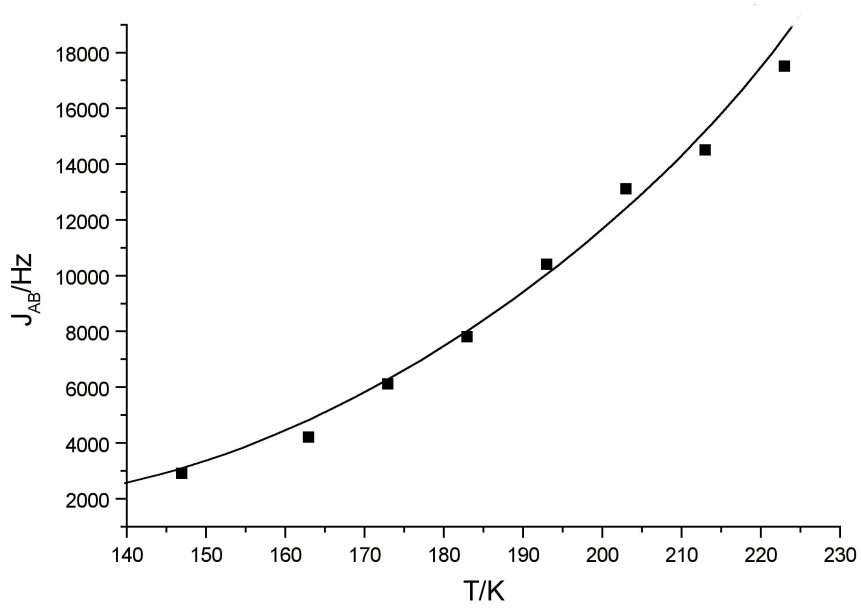

Figure 4.6 Variation of J_{AB} with temperature for the compound $[W\{(\eta-C_5H_4)C(C_5H_{10})(\eta-C_5H_4)\}H_3][BF_4]$ **(37)**

Experiments have been undertaken to attempt to further probe the nature of this quantum mechanical exchange coupling phenomenon in *ansa*-metallocene trihydride complexes. Exchange couplings have been shown to be very sensitive to slight modifications of the hydride environment and of the electron density at the metal centre. For example in the series of compounds $[Nb(\eta-C_5H_3RR')_2H_3]$ (R, R' = H or $SiMe_3$) J_{AB} is found to be largest in the compound $[Nb\{\eta-C_5H_3(SiMe_3)_2\}_2H_3]$. Exchange coupling is further increased on addition of Lewis acidic coinage cationic species such as $[Cu(MeCN)_4][PF_6]$ or $AgBF_4$.[18]

In light of recent reports by Crabtree of the existence of dihydrogen bonds (H---H hydrogen bonds) between a hydride ligand and a proton of an organic molecule,[19, 20] Chaudret has examined the spectroscopic properties of the compounds $[Ru(\eta-C_5M_4)(PCy_3)H_3]$ (R = cyclohexyl) in the presence of various proton donors such as indole, p-CF_3-phenol and hexafluoro-2-propanol.[21] The hydrogen bond donor is found to interact preferentially with the central hydrogen atom while as much as a threefold increase in J_{AB} is observed. The magnitude of the exchange coupling is related to the hydrogen bond donor ability and the increase in J_{AB} in the presence of such proton donors

has been rationalised in terms of a reduction in M-H bond strength facilitating close approach of exchanging hydrogens.

In this study variable temperature ^{1}H NMR spectra of the compound **37** show no discernible change in the high field region of the spectra in the presence of the proton donor p-CF_3-phenol. Within experimental error J_{AB} is found to be unchanged by the addition of p-CF_3-phenol even as the concentration of the proton donor is increased. The apparent absence of a hydrogen bond interaction between the compound **37** and p-CF_3-phenol is perhaps not surprising given that the compound **37** is an ionic species. Attempts to determine J_{AB} in the presence of indole were thwarted as this species was found to react with the compound **37.**

Whereas $[W(\eta\text{–}C_5H_5)_2H_3]^+$ exhibits normal behaviour in the ^{1}H NMR spectra the analogous second row compound $[Mo(\eta\text{–}C_5H_5)_2H_3]^+$ displays quantum mechanical exchange coupling with J_{AB} increasing from 450 Hz at 153 K to 1000 Hz at 203 K.[7] In the light of these observations and the magnitude of J_{AB} for one carbon-bridged tungstenocene trihydride cations, attempts were made to protonate the *ansa*-molybdocene dihydride compound $[Mo\{(\eta\text{–}C_5H_4)CMe_2(\eta\text{–}C_5H_4)\}H_2]$. However the corresponding trihydride $[Mo\{(\eta\text{–}C_5H_4)CMe_2(\eta\text{–}C_5H_4)\}H_3]^+$ was not isolated nor detected spectroscopically. Density functional calculations show that the ground state structure of $[Mo\{(\eta\text{–}C_5H_4)CMe_2(\eta\text{–}C_5H_4)\}H_3]^+$ is a dihydrogen hydride $(\eta^2\text{-}H_2)H$ species rather than a classical trihydride.[22] This species is expected to be thermally unstable. Attempts to observe the compound $[Mo\{(\eta\text{–}C_5H_4)CMe_2(\eta\text{–}C_5H_4)\}H_3]^+$ spectroscopically at very low temperatures are ongoing in collaboration with Professor D. M. Heinekey of the University of Washington, Seattle.

A potentially exciting experiment to study the thermal motions of the hydride ligands within the compound **37** *via* single crystal neutron diffraction at a range of temperatures is planned. This new technique, pioneered in the Isis Facility at the Rutherford Appleton Laboratory, Oxon., has successfully modelled the thermal motions of hydrogen atoms in a number of interesting compounds. For example the temperature dependence of hydrogen-atom disorder in benzoic acid dimers has been studied.[23, 24] Thus much attention has focussed on obtaining single crystals of the compound **37** suitable for neutron structure determination. Recrystallisation from a variety of polar solvents has been attempted and efforts are ongoing. Attempts to study the low energy bending motions of the hydride ligands in the compound **37** by Inelastic Neutron

Spectroscopy were made. However this experiment proved unsuccessful due to an inability to obtain spectra of sufficient quality. Ideally a multigram quantity of compound is required for such an experiment.

4.2.6 Preparation of [W{(η–C_5H_4)C_2Me_4(η–C_5H_4)}Me_2] (38)

Some chemistry of Group 6 *ansa*-metallocenes in which the cyclopentadienyl rings are bridged by the tetramethylethylene unit C_2Me_4 has been explored previously in this laboratory.[2, 25] The trihydride species [W{(η–C_5H_4)C_2Me_4(η–C_5H_4)}H_3][Cl] displays quantum mechanical exchange coupling in its ^{1}H NMR spectra. As has been described in **Section 4.2.1** and is described in **Section 4.2.7** the magnitude of the exchange coupling has been shown to vary with the geometry of the metallocene unit. Attempts to obtain crystals suitable for X-ray molecular structure determination of the compound [W{(η–C_5H_4)C_2Me_4(η–C_5H_4)}H_3][Cl] were unsuccessful. Therefore in order to obtain important structural parameters of this class of *ansa*-metallocene the compound [W{(η–C_5H_4)C_2Me_4(η–C_5H_4)}Me_2] **(38)** was prepared by the action of $ZnMe_2$ on a suspension of the compound [W{(η–C_5H_4)C_2Me_4(η–C_5H_4)}Cl_2] in toluene at low temperature (**Scheme 4.5**). Following hydrolysis of excess $ZnMe_2$ the compound **38** was recrystallised from a concentrated pentane solution at -80 ºC and obtained as an orange powder.

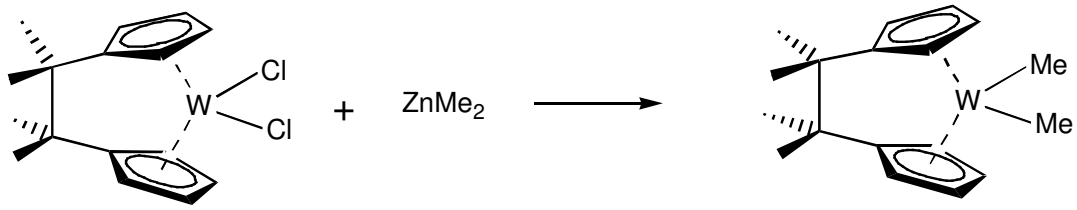

38

Scheme 4.5 Preparation of [W{(η–C_5H_4)C_2Me_4(η–C_5H_4)}Me_2] **(38)**

The compound **38** was characterised by FAB mass spectrometry and ^{1}H and ^{13}C NMR spectroscopy. The FAB mass spectrum of the compound **38** shows peaks due to the molecular ion and fragmentation products arising from the sequential loss of the methyl ligands. The ^{1}H and ^{13}C{^{1}H} NMR spectra of the compound **38** are straightforward and not discussed further here.

Further purification of the compound **38** was afforded by passage in toluene/pentane down a chromotography column packed with activated alumina. Removal of volatiles under reduced pressure yielded an orange powder. Slow cooling of a concentrated solution of the resulting residue in pentane to -80 °C afforded single crystals of the compound **38** suitable for X-ray molecular structure determination. The crystal structure was determined and the molecular structure is shown in **Figure 4.7**. Selected interatomic distances and angles and other structural information are presented in **Table 4.4**. Full details of the molecular structure determination are given in **Appendix G**. The compound crystallises in the triclinic space group PI.

Structural parameters for the compound **38** and other *ansa*-tungstenocene dimethyl compounds are compared in **Table 4.5**. The molecular structure of the nonbridged compound $[W(\eta\text{–}C_5H_5)_2Me_2]$ has not been reported. The tetramethylene bridge does not exert such a dramatic influence on the geometry of the *ansa*-metallocene fragment as the single carbon bridge in the analogous compounds **35** and $[W\{(\eta\text{–}C_5H_4)CMe_2(\eta\text{–}C_5H_4)\}Me_2]$. The bending angle β in the compound **38** is *ca*. 10º larger than in the compound **35**. The increased bending of the rings in the single-carbon bridged compounds corresponds to a significant decrease in the C_{ipso}-C_{ipso} distance. The effect on the metallocene geometry imparted by an ethylene- and silicon-bridge is again seen to be similar.

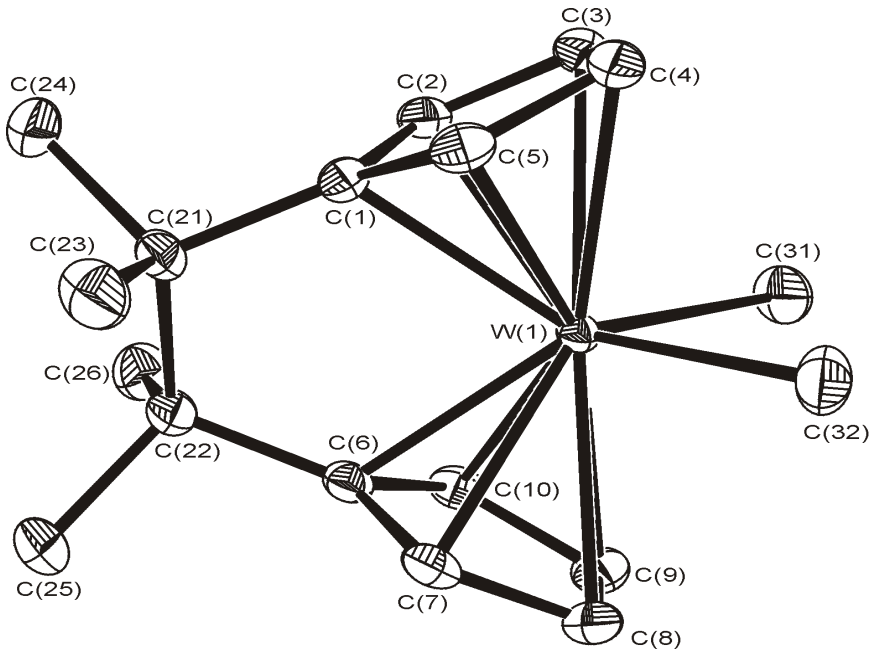

Figure 4.7 Molecular structure of $[W\{(\eta\text{–}C_5H_4)C_2Me_4(\eta\text{–}C_5H_4)\}Me_2]$ **(38)**
Hydrogen atoms are omitted for clarity.

	Length / Å		Angle / °
W-Cp^1_{cent}	1.961(3)	Between Cp planes, α	50.9
W-Cp^1_{ave}	2.305	Cp^1_{norm}-W-Cp^2_{norm}, β	129.1
W-Cp^2_{cent}	1.954(3)	Cp^1_{cent}-W-Cp^2_{cent}, χ	136.6
W-Cp^2_{ave}	2.300	C_{ipso}-Cp plane, ϕ	17.6, 18.8
W-C(1)	2.236(3)	C(31)-W-C(32)	77.76(11)
W-C(3)	2.372(3)		
W-C(31)	2.246(2)		

Cp^1 = Ring C(1)-C(5), Cp^2 = Ring C(6)-C(7)

Table 4.4 Selected interatomic distances and angles and other structural information for $[W\{(\eta\text{–}C_5H_4)C_2Me_4(\eta\text{–}C_5H_4)\}Me_2]$ **(38)**

Bridging unit E	α (°)	β (°)	γ (°)	C_{ipso}-C_{ipso} (Å)	Reference
C_2Me_4 **(38)**	50.9	129.1	136.6	2.606	*a*
$SiMe_2$	50.4	129.6	138.1	2.660	2
CMe_2	60.9	119.1	128.4	2.273	3
$C(C_5H_{10})$ **(35)**	61.7	118.3	127.6	2.249	*a*

[a] This work

Table 4.5 Structural parameters for the compounds $[W\{(\eta-C_5H_4)E(\eta-C_5H_4)\}Me_2]$

4.2.7 Theoretical Study of the Effect of an *ansa*-Bridge on the Energy Barrier to Hydrogen Exchange

As described in **Section 4.2.1** two key features of the model proposed for quantum mechanical exchange coupling in polyhydrides are the ease of close approach of the exchanging hydrogens and the size of the barrier to classical exchange, which should lie between 35 and 70 kJ mol^{-1} for the phenomenon to be observable by ^1H NMR spectroscopy. The exchange pathway in nonbridged, silicon-bridged and one-carbon bridged trihydrides has been studied theoretically by Green and Scottow.[26] Their work is discussed briefly in this section to provide a fuller picture of the overall progress in this area and to help to understand the experimental observations described in the preceding sections of this chapter. The backbone of the *ansa*-bridge was simplified to save computational time with calculations performed on the cations $[W(\eta-C_5H_5)_2H_3]^+$ **(I)**, $[W\{(\eta-C_5H_4)SiH_2(\eta-C_5H_4)\}H_2]^+$ **(II)** and $[W\{(\eta-C_5H_4)CH_2(\eta-C_5H_4)\}H_3]^+$ **(III)** (**Figure 4.8**).

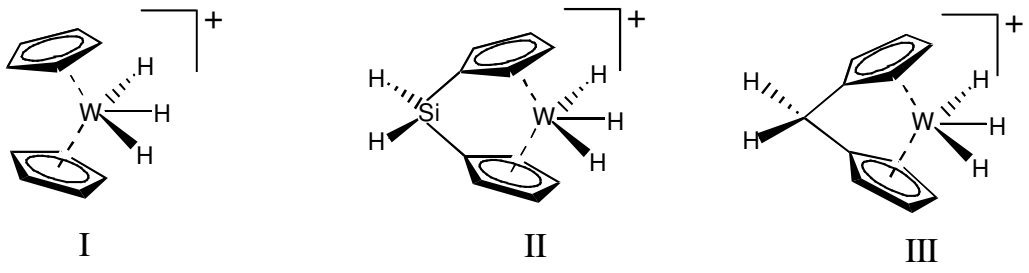

Figure 4.8 The trihydride cations used in the density functional calculations

The mid-point of the exchange process was assumed to be an (η^2-H_2)H structure **c** with the H-H axis perpendicular to the xz plane (**Figure 4.9**). The ease of approach of the exchanging hydrogens within the xz plane was studied by calculating the energy of a structure **b** as the H_b-W-H_a angle was varied. The energy difference between the structure **b** (θ = 31°) and the minimum energy structure **a** shows that the ease of approach of the exchanging hydrogens increases with increasing inter-ring angle α and decreasing bending angle β from **I** to **II** to **III** (**Table 4.6**). Furthermore the energy differences between the minimum energy structures and the mid-point **c** show a decrease from 96 kJmol^{-1} for **I** to 63 kJmol^{-1} for **II** to 51 kJmol^{-1} for **III**. Thus the exchange energy barriers for **II** and **III** are calculated to lie in the 35-70 kJmol^{-1} region within which quantum mechanical exchange coupling can be observed by ^{1}H NMR spectroscopy. The compounds $[W\{(\eta\text{-}C_5H_4)SiMe_2(\eta\text{-}C_5H_4)\}H_3]^+$ and $[W\{(\eta\text{-}C_5H_4)CMe_2(\eta\text{-}C_5H_4)\}H_3]^+$ do indeed exhibit exchange coupling. The lower barrier for **III** compared to **II** is consistent with the greater magnitude of J_{AB} in the one-carbon bridged compounds **38** and $[W\{(\eta\text{-}C_5H_4)CMe_2(\eta\text{-}C_5H_4)\}H_3]^+$ compared to the geometrically less constrained silicon-bridged species $[W\{(\eta\text{-}C_5H_4)SiMe_2(\eta\text{-}C_5H_4)\}H_3]^+$ and $[W\{(\eta\text{-}C_5H_4)C_2Me_4(\eta\text{-}C_5H_4)\}H_3]^+$. The barrier to exchange is calculated to be greater than 70 kJmol^{-1} for **I** and $[W(\eta\text{-}C_5H_5)_2H_3]^+$ is found to exhibit temperature independent coupling with J_{AB} = 8.5 Hz.

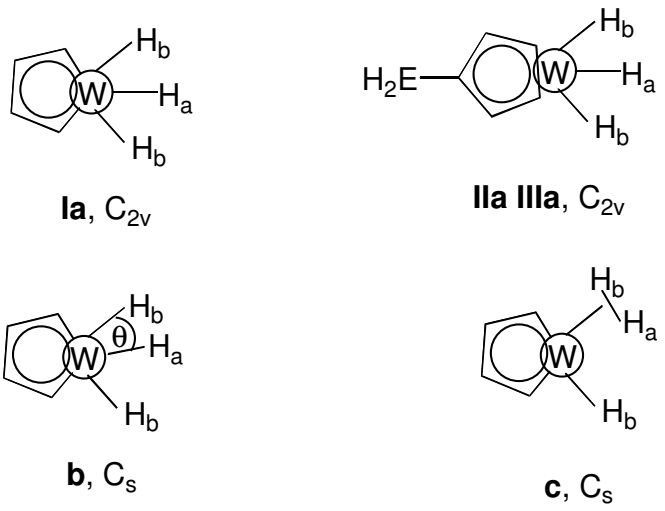

Figure 4.9 Structures and symmetries assumed for the metallocene trihydride cations **I-III** in the calculations of the ground state **a**, the WH_2 bend **b** and the mid-point of the H_a-H_b exchange **c**

	I	**II**	**III**
b / $kJmol^{-1}$	30.2	15.0	6.8
c / $kJmol^{-1}$	95.5	62.5	51.3
α / °	29	48	62
β / °	151	132	118

Table 4.6 Calculated energies of structures **b** (θ = 31°) and **c** relative to **a** and the inter-ring angle α and bending angle β in the structure **a** for the trihydrides **I-III**

As the inter-ring angle α increases and the corresponding bending angle β decreases as the *ansa*-bridge becomes more constraining, a lengthening of the W-H bonds is observed, while the W-H atom-atom overlap population decreases from **I** to **II** to **III**. The frontier orbitals of a metallocene unit superimposed on a plan of the trihydride structure are shown in **Figure 4.10**. Green has previously shown that as the inter-ring angle α is increased the $4a_1$ and $2b_1$ orbitals rise in energy, with the $4a_1$ orbital rising particularly steeply (**Section 1.1.2**).[27] This orbital is best oriented to bind the central hydrogen. As the rings are bent the metal $d(z^2\text{-}y^2)$ orbital becomes more involved in

bonding to the cyclopentadienyl π system and the $4a_1$ orbital is the antibonding orbital of this bonding interaction. Thus the further bending of the rings imparted by an *ansa*-bridge decreases the binding of the hydride ligands, particularly the central hydride. Hydrogen exchange is more easily accessed and the magnitude of exchange coupling is increased.

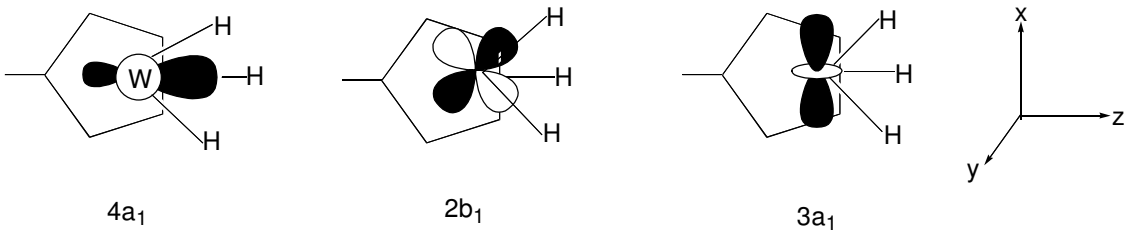

Figure 4.10 Frontier orbitals of a bent metallocene unit superimposed on a trihydride structure

It is also instructive to consider the change in the formal oxidation state of the metal on forming the W(η^2-H_2)H transition state, **c**, from the WH_3 ground state **a**. This constitutes a formal reduction of the metal from +6 to +4 i.e. the electron configuration changes from d^0 to d^2. This involves occupying the $3a_1$ orbital which is stabilised as the inter-ring angle α is increased (**Section 1.1.2**). Thus the increased ease of forming the transition state with increase in inter-ring angle may also be due in part to the increase in stability of this orbital on bending of the rings

4.3 Quantum Mechanical Exchange Coupling in Niobocene Trihydrides

4.3.1 Introduction

The nonbridged niobocene trihydride [Nb(η−$C_5H_5)_2H_3$] has been shown to exhibit novel behaviour in the ^{1}H NMR spectra.[7] Firstly the compound undergoes quantum mechanical exchange coupling with J_{AB} decreasing from 20 Hz at 303 K to 4.5 Hz at 253 K. The coupling pattern becomes unresolvable below this temperature but unexpectedly reappears at 173 K. Since the observed coupling J_{AB} is given by the equation $J_{AB} = J_m - 2J_{ex}$ and J_{ex} is predicted by theory to be negative, the presence of an exchange coupling component is expected to lead to a positive contribution to J_{AB} (**Section 4.2.1**). However if the sign of J_m is also negative it may cancel out the positive contribution due to exchange coupling if J_m and J_{ex} are comparable in magnitude. Since J_{ex} is temperature

dependent this situation would be indicated by a temperature dependent J_{AB} which would decrease with decreasing temperature, go through zero and then increase again as the temperature is lowered further.

In the light of the interesting behaviour of $[Nb(\eta-C_5H_5)H_3]$ and the significant changes in the spectroscopic properties of metallocene trihyrides upon the introduction of an *ansa*-bridge as described in **Sections 4.2.5** and **4.2.7** it was decided to explore the properties of *ansa*-niobocene trihydrides. Significant efforts in this laboratory had previously been focussed on the preparation of the one carbon-bridged compound $[Nb\{(\eta-C_5H_4)CMe_2(\eta-C_5H_4)\}H_3]$.[28] However a variety of synthetic approaches proved to be unsuccessful. Thus the preliminary investigations into *ansa*-niobocene trihydride chemistry described in this work were carried out on silicon- and ethylene-bridged compounds where the effect of the ansa-bridge on the structural and electronic properties have been shown to be less marked.

4.3.2 Reaction between $[Nb\{(\eta-C_5H_4)E(\eta-C_5H_4)\}Cl_2]$ (E = $SiMe_2$, C_2Me_4 (1)) and $[Na\{AlH_2(OCH_2CH_2OCH_3)_2\}]$

Labinger and Schwartz have described the preparation of the compound $[Nb(\eta-C_5H_5)_2H_3]$ *via* the addition of $[Na\{AlH_2(OCH_2CH_2OCH_3)_2\}]$ to a toluene suspension of $[Nb(\eta-C_5H_5)Cl_2]$ at low temperature.[29] Treatment of the compound $[Nb\{(\eta-C_5H_4)SiMe_2(\eta-C_5H_4)\}Cl_2]$ with a solution of $[Na\{AlH_2(OCH_2OCH_2CH_3)_2\}]$ in toluene at -78 ºC prior to cautious hydrolysis of excess $[Na\{AlH_2(OCH_2CH_2OCH_3)_2\}]$, removal of volatiles and washing with ethanol, affords a pale brown solid. ^{1}H NMR spectroscopy of this residue reveals the presence of the compound $[Nb\{(\eta-C_5H_4)SiMe_2(\eta-C_5H_4)\}H_3]$. Two partial triplets at δ 4.96 and 4.88 ppm are assigned to the protons of the cyclopentadienyl rings. A singlet at δ 0.38 ppm is assigned to the protons of $SiMe_2$ bridge. A triplet at δ -2.95 ppm and doublet at δ -3.92 ppm are assigned to the one H_A and two H_B protons of an AB_2 system respectively. Associated with the compound were unidentified impurities in the δ 1-3 ppm region of the spectrum.

Despite repeated attempts, isolation of the compound $[Nb\{(\eta-C_5H_4)SiMe_2(\eta-C_5H_4)\}H_3]$ was not achieved, consistently being thwarted by the low yield of compound obtained. An alternative synthetic strategy involving bubbling dihydrogen through a solution of the compound

$[Nb\{(\eta-C_5H_4)SiMe_2(\eta-C_5H_4)\}\{\eta^2-BH_4\}]$ **(6)** in toluene in the presence of pyridine failed to yield any tractable products. Such a procedure has been successfully employed to prepare the compound $[Nb(\eta-C_5H_5)_2H_3]$.[30]

High field variable temperature ^1H NMR spectra of the compound $[Nb\{(\eta-C_5H_4)SiMe_2(\eta-C_5H_4)\}H_3]$ in $C_6D_5CD_3$ are shown in **Figure 4.11**. At 303 K J_{AB} is 68 Hz and marks a threefold increase compared to the highest value of J_{AB} found for the analogous nonbridged compound $[Nb(\eta-C_5H_5)H_3]$. As the temperature is lowered J_{AB} can be seen to decrease. At 243 K J_{AB} is reduced to 6 Hz and the coupling pattern becomes unresolvable as the temperature is reduced further. Decreasing the temperature down to 173 K shows no evidence of J_{AB} increasing, with the coupling pattern remaining unresolvable.

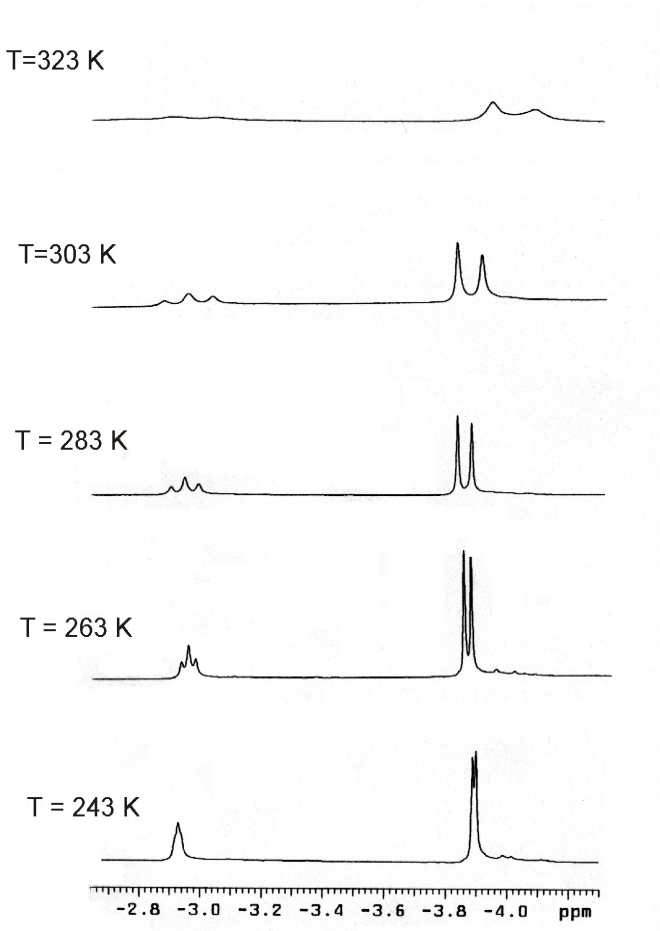

Figure 4.11 High field variable temperature ^1H NMR spectra of the compound $[Nb\{(\eta-C_5H_4)SiMe_2(\eta-C_5H_4)\}H_3]$

Treatment of the ethylene-bridged compound $[Nb\{(\eta-C_5H_4)C_2Me_4(\eta-C_5H_4)\}Cl_2]$ **(1)** with $[Na\{AlH_2(OCH_2OCH_2CH_3)_2\}]$ allows the identification of

$[Nb\{(\eta-C_5H_4)C_2Me_4(\eta-C_5H_4)\}H_3]$ by ^1H NMR spectroscopy. Again isolation of an authentic sample was not possible due to the extremely low yield of the product. In the high field region of the room temperature ^1H NMR spectrum two broad peaks at δ -1.22 and -1.58 ppm are observed. On cooling to 243 K these broad peak sharpen and split into a triplet at δ -0.44 ppm and a doublet at δ -1.72 ppm and are thus assigned to the H_A and H_B protons respectively. As the temperature is reduced further the ^1H NMR spectra reveal a temperature dependent coupling constant J_{AB}. Values of J_{AB} are compared to J_{AB} for the compounds $[Nb\{(\eta-C_5H_4)SiMe_2(\eta-C_5H_4)\}H_3]$ and $[Nb\{(\eta-C_5H_5)_2H_3]$ in **Table 4.7**. A plot of J_{AB} against temperature for these three compounds is shown in **Figure 4.12.** All three compounds shows a exponential-like increase of J_{AB} with temperature.

T/K	J_{AB}/Hz		
	$[Nb(\eta-C_5H_5)_2H_3]$[7]	E = $SiMe_2$	E = C_2Me_4
323		60.0	
313		48.5	
303	20.4	41.5	
293	13.6	31.0	
283	11.0	24.5	
273	9.8	17.5	
263	7.1	12.0	
253	4.5	7.0	
243	-	6.5	100.0
233	3.4		60.0
223			36.0
213			19.5
203			15.5
193	5.9		7.5

Table 4.7 Values of J_{AB} derived from variable temperature ^1H NMR spectroscopy of the compounds $[Nb(\eta-C_5H_5)_2H_3]$ and $[Nb\{(\eta-C_5H_4)E(\eta-C_5H_4)\}H_3]$ (E = C_2Me_4, $SiMe_2$)

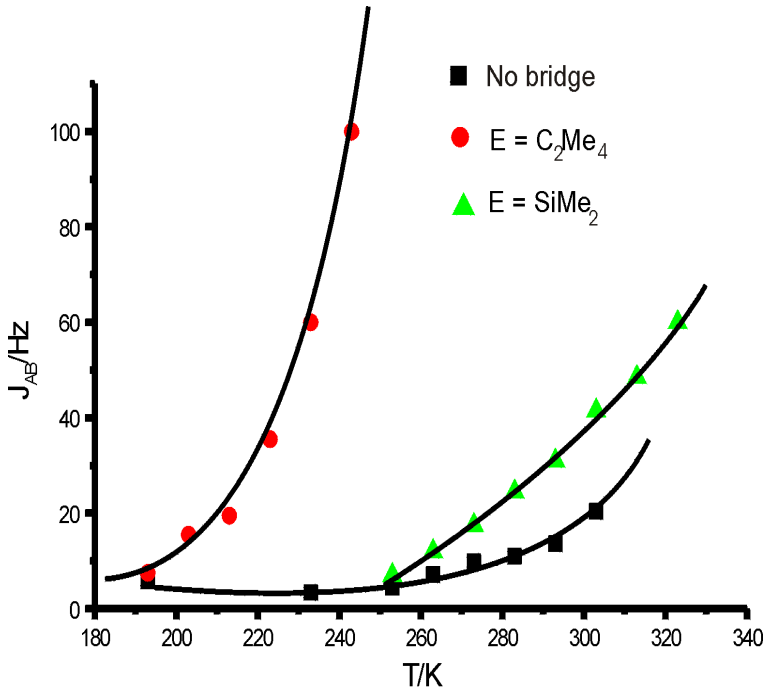

Figure 4.12 Variation of J_{AB} with temperature for the compounds

$[Nb(\eta\text{–}C_5H_5)_2H_3]$ + and $[Nb\{(\eta\text{–}C_5H_4)E(\eta\text{–}C_5H_4)\}H_3]$ (E = C_2Me_4 &, $SiMe_2$ △)

The introduction of an *ansa*-bridge is seen to increase the magnitude of J_{AB} compared to analogous nonbridged trihydrides at equivalent temperatures. The effect is most marked for the ethylene-bridged compound $[Nb\{(\eta\text{–}C_5H_4)C_2Me_4(\eta\text{–}C_5H_4)\}H_3]$ where J_{AB} = 100 Hz at 243 K. The fact that the magnitude of J_{AB} and hence J_{ex} for the compounds $[Nb\{(\eta\text{–}C_5H_4)C_2Me_4(\eta\text{–}C_5H_4)\}H_3]$ and $[Nb\{(\eta\text{–}C_5H_4)SiMe_2(\eta\text{–}C_5H_4)\}H_3]$ is markedly different illustrates that subtle changes in geometry of the metallocene unit can have a significant effect on the exchange coupling. Indeed by analogy to the molecular structures of the compounds $[Nb\{(\eta\text{–}C_5H_4)C_2Me_4(\eta\text{–}C_5H_4)\}\{\eta^2\text{–}BH_4\}]$ **(2)** and $[Nb\{(\eta\text{–}C_5H_4)SiMe_2(\eta\text{–}C_5H_4)\}\{\eta^2\text{–}BH_4\}]$ **(6)** (**Section 2.5.3**) the inter-ring angle α and bending angle β in the compounds $[Nb\{(\eta\text{–}C_5H_4)C_2Me_4(\eta\text{–}C_5H_4)\}H_3]$ and $[Nb\{(\eta\text{–}C_5H_4)SiMe_2(\eta\text{–}C_5H_4)\}H_3]$ are expected to be similar.

The low yields and isolation problems associated with the compounds $[Nb\{(\eta\text{–}C_5H_4)C_2Me_4(\eta\text{–}C_5H_4)\}H_3]$ and $[Nb\{(\eta\text{–}C_5H_4)SiMe_2(\eta\text{–}C_5H_4)\}H_3]$ and the inaccessibility of the compound $[Nb\{(\eta\text{–}C_5H_4)CMe_2(\eta\text{–}C_5H_4)\}H_3]$ can be understood in the light of a recent study of *ansa*-tantalocene trihydrides by Parkin *et al.* (**Section 1.5.2**).[31] A comparison of the chemistry of $[Ta\{(\eta\text{–}C_5Me_4)SiMe_2(\eta\text{–}C_5Me_4)\}H_3]$ and

$[Ta\{(\eta-C_5Me_4)SiMe_2(\eta-C_5Me_4)\}(\eta^2-C_2H_4)H]$ with their nonbridged permethyltantalocene counterparts demonstrated that the incorporation of a silicon-bridge substantially increases the rates of both reductive elimination of H_2 and ethylene insertion into a Ta-H bond. The compound $[Ta\{(\eta-C_5Me_4)SiMe_2(\eta-C_5Me_4)\}H_3]$ reacts with ethylene *ca*. 4000 times faster than $[Ta(\eta-C_5Me_5)_2H_3]$.

4.4 Preliminary Investigations into *ansa*-Rhenocene Chemistry

4.4.1 Introduction

The cationic rhenocene alkyl hydrides $[Re(\eta-C_5H_5)_2R(H)]^+$ are highly labile, undergoing alkane elimination even at low temperatures.[32, 33] Since the fragments $[W(\eta-C_5H_5)_2]$ and $[Re(\eta-C_5H_5)_2]^+$ are isoelectronic and by analogy with $[W\{(\eta-C_5H_4)CMe_2(\eta-C_5Me_4)\}(Me)H]$ it is anticipated that the stability of rhenocene alkyl hydrides with respect to reductive elimination might be increased by the introduction of a single carbon *ansa*-bridge.

During the course of this work Heinekey has described the first *ansa*-rhenocene compounds.[34] The parent compound $[Re\{(\eta-C_5H_4)SiMe_2(\eta-C_5H_4)\}Me]$ was prepared in high yield by the lithiation of the cyclopentadienyl rings of $[Re(\eta-C_5H_5)_2Me]$ using ^nBuLi, followed by reaction with Me_2SiCl_2, presumably *via* the dianionic intermediate $[Re(\eta-C_5H_4)_2Me][Li_2]$. Attempts to access the carbon-bridged compound $[Re\{(\eta-C_5H_4)CMe_2(\eta-C_5H_4)\}Me]$ in an analogous procedure were unsuccessful. Preliminary investigations have shown that the silicon-bridged species $[Re\{(\eta-C_5H_4)SiMe_2(\eta-C_5H_4)\}Me(H)]^+$ displays increased thermal stability relative to the nonbridged analogue.

It was decided to attempt to prepare single carbon-bridged *ansa*-rhenocene complexes. Synthetic investigations were carried out in collaboration with Dr. A. H. H. Stephens of this laboratory.

4.4.2 Preparation of [Re{(η–C_5H_4)CMe_2(η–C_5H_4)}Cl] (39)

A procedure analogous to that described for the preparation of the non-bridged rhenocene compound [Re(η–C_5H_5)$_2$Cl] was used to prepare the compound [Re{(η–C_5H_4)CMe_2(η–C_5H_4)}Cl] **(39)** (**Scheme 4.6**). Addition of excess [K_2{(C_5H_4)CMe_2(C_5H_4)}] to $ReCl_5$ in DME at low temperature followed by extraction into THF and then dichloromethane gives crude **39** as a red-brown solid in 10 % yield. An analytically pure sample of the compound **39** was obtained by recrystallisation from a dichloromethane solution in a final yield of *ca.* 3%.

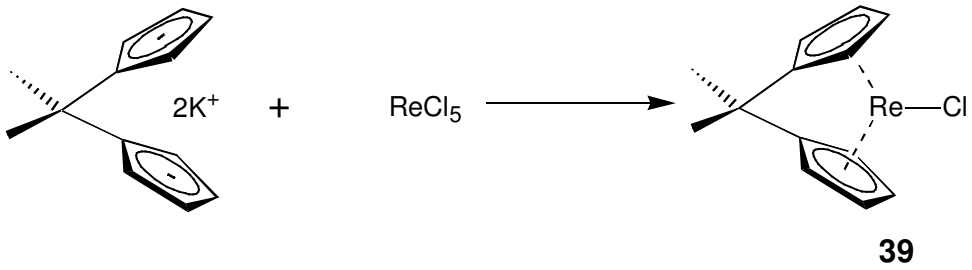

39

Scheme 4.6 Preparation of [Re{(η–C_5H_4)CMe_2(η–C_5H_4)}Cl] **(39)**

The low yield of the compound **39** is not unexpected in the light of our experience in the synthesis of Group 6 *ansa*-metallocenes and the low yielding synthesis of non-bridged rhenocene complexes.[32, 33, 35] Considerable effort was focussed on improving the yield of the compound **39** in order to facilitate a full study of its chemistry. Reaction conditions were varied and alternative reagents employed. The compound **39** was prepared by the reaction between $ReCl_5$ and [Li_2{(C_5H_4)CMe_2(C_5H_4)}] and between $ReCl_4$.2THF and [K_2{(C_5H_4)CMe_2(C_5H_4)}] although the product yield proved to be as disappointing as in the reaction described above. The reaction between $ReCl_5$ and [Li_2{(C_5H_4)CMe_2(C_5H_4)}] in the presence of $NaBH_4$ was performed in an attempt to prepare the compound [Re{(η–C_5H_4)CMe_2(η–C_5H_4)}H]. However no tractable product was obtained from this reaction. Attempts to prepare the ethylene-bridged compound [Re{(η–C_5H_4)C_2Me_4(η–C_5H_4)}Cl] were not successful.

The compound **39** was characterised by elemental analysis, FAB mass spectrometry and ^{1}H and ^{13}C{^{1}H} NMR spectroscopy. The FAB mass spectrum of the compound **39** shows peaks due to the molecular ion and a fragmentation product due to the loss of the chloride ligand. The ^{1}H NMR spectrum of the compound **39** consists of

two partial triplets at δ 5.29 and 4.36 ppm corresponding to the two sets of cyclopentadienyl protons and a singlet at δ 0.99 ppm due to the protons of the CMe_2 bridge. The $^{13}C\{^1H\}$ NMR spectrum of the compound **39** shows peaks at δ 83.8 and 76.1 ppm due to the carbons of the cyclopentadienyl rings. Two quaternary carbons are located at δ 34.4 and 31.6 ppm and are assigned to the *ipso*-carbon and CMe_2 bridgehead carbon while a singlet at δ 22.1 ppm corresponds to the methyl carbons of the bridging unit.

Slow cooling of a concentrated solution of the compound **39** in dichloromethane to -80 °C afforded single crystals suitable for X-ray structural analysis. The crystal structure was determined and the molecular structure is shown in **Figure 4.13**. Selected interatomic distances and angles and other structural information are presented in **Table 4.8**. Full details of the molecular structure determination are given in **Appendix H**. The compound crystallises in the monoclinic space group $P2_1/c$.

The bending angle β = 126.9° is much reduced compared to the non-bridged analogue $[Re(\eta\text{–}C_5H_5)_2Cl]$ (β = 139.8°) and indicates great strain is imparted by the CMe_2 bridge.[35] In contrast, the bending angle β in the silicon-bridged species $[Re\{(\eta\text{–}C_5H_4)SiMe_2(\eta\text{–}C_5H_4)\}Me]$ (β = 140.0°) is close to that typically found in non-bridged rhenocene compounds.[34] The CMe_2 bridge imposes a significant distortion from planarity at the *ipso*-carbon (ϕ = 20.9° and 22.0°). The Re-C(1) and Re-C(6) distances are the shortest Re-C distances as the metal is pulled towards the *ipso*-carbon. The presence of one particularly short ring C-C bond, as evidenced by ΔCp^1 = 0.04125 Å, suggests that the bonding mode of the η-cyclopentadienyl rings is partially η^3 in character (**Section 4.2.3**).

Of particular note in the molecular structure is the angle θ defined by the C(11)...Re vector and the Cl atom which is found to have a value of 170.4° (**Figure 4.14**). A value much closer to 180° is expected. This phenomenon is not seen in other rhenocene derivatives. For instance in the non-bridged analogue $[Re(\eta\text{–}C_5H_5)_2Cl]$ where the rings are slightly staggered, a point X can be defined at the centroid of the four carbon atoms furthest from the Cl atom. The angle X...Re-Cl is found to be 179.4°.[35] As a result of the Re-Cl bond being displaced from the C(11)..Re vector in the compound **39** the rings are slightly canted with the side to which the chlorine atom lies becoming more open. The C(2)-C(7) distance is 0.194 Å longer than the C(5)-C(10) distance and the C(3)-C(8) distance 0.106 Å longer than the C(4)-C(9) distance.

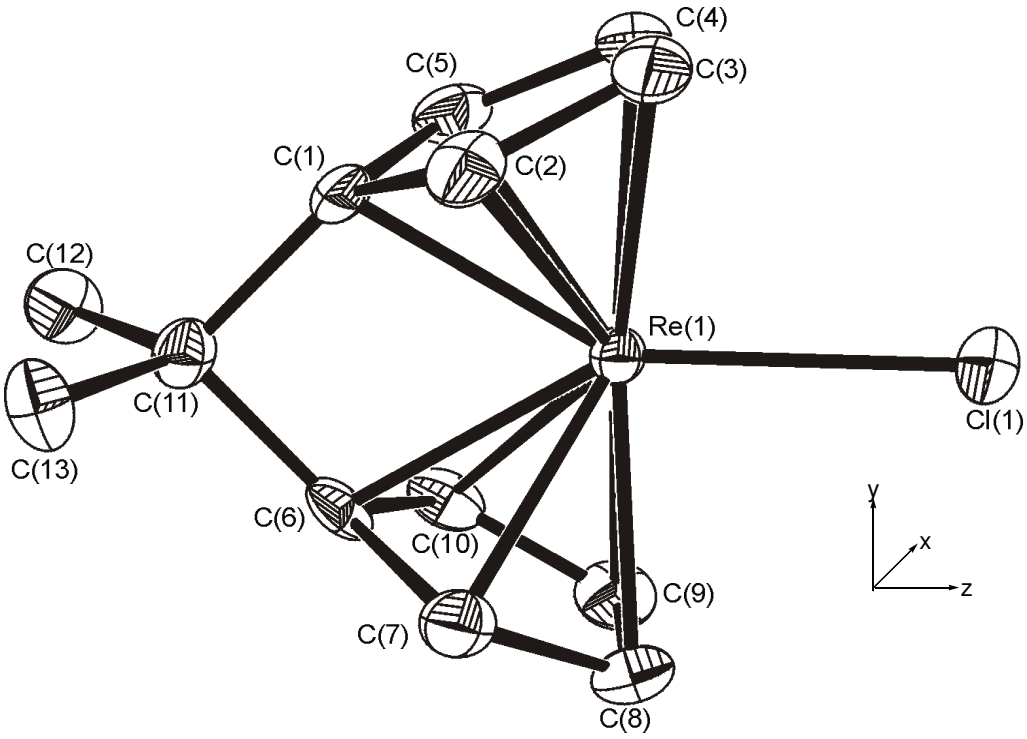

Figure 4.13 Molecular structure of [Re{(η–C_5H_4)CMe_2(η–C_5H_4)}Cl] **(39).** Hydrogen atoms are omitted for clarity

	Length / Å		Angle / °
Re-Cp^1_{cent}	1.8529	Between Cp planes, α	53.1
Re-Cp^1_{ave}	2.2164(5)	Cp^1_{norm}-Re-Cp^2_{norm}, β	126.9
Re-Cp^2_{cent}	1.8577	Cp^1_{cent}-Re-Cp^2_{cent}, χ	131.3
Re-Cp^2_{ave}	2.2206(5)	C_{ipso}-Cp plane, ϕ	20.9, 22.0
Re-C(1)	2.175(5)	C(1)-C(11)-C(6), ε	95.8(4)
Re-C(3)	2.245(5)	C(11)...Re-Cl, θ	170.4
Re-Cl	2.4383(13)		
ΔCp^1	0.04125(7)		

Cp^1 = Ring C(1)-C(5), Cp^2 = Ring C(6)-C(10)

Table 4.8 Selected interatomic distances and angles and other structural information for [Re{(η–C_5H_4)CMe_2(η–C_5H_4)}Cl] **(39)**

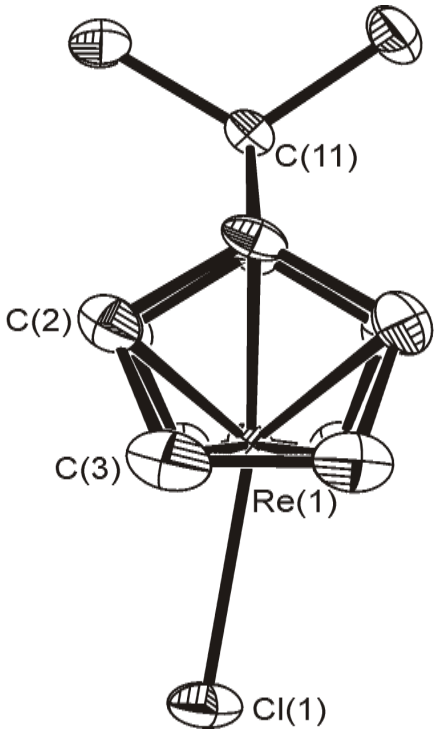

Figure 4.14 Alternative view of the molecular structure of $[Re\{(\eta-C_5H_4)CMe_2(\eta-C_5H_4)\}Cl]$ **(39).** Hydrogen atoms are omitted for clarity

4.3.2 Density Functional Calculations

Whilst the possibility of crystal packing effects on molecular geometry determined by single crystal X-ray diffraction is always present, the unexpected molecular structure of the compound **39** was of some interest. Theoretical predictions using density functional calculations have had success in accounting for some of the properties of *ansa*-bridged compounds.[26, 27, 36, 37] As described for the metallocene trihydrides in **Section 4.2.7**, when the rings are bridged by a single carbon unit, binding of the metal to the *ipso*-carbons is strengthened at the expense of a centrally bound additional ligand, i.e. H_A.[26, 38] It seemed likely that similar factors might be responsible for the displacement of the chlorine atom from the central position in the compound **39**.

As for the study of the structural and dynamic properties of niobocene tetrahydroborate derivatives described in **Section 2.6**, density functional calculations were performed by Professor J. C. Green and her research group in the light of the experimental observations made during this work. These calculations provide an explanation for the unexpected molecular structure of the compound **39**. A summary of the density functional

calculations carried out by Professor Green and her group and the conclusions which are drawn are presented in this section.

In order to understand the origin of the unsymmetrical structure of the compound **39** density functional calculations were carried out on [Re{(η–C_5H_4)CH_2(η–C_5H_4)}Cl] **(II)** as a model for **39** and the nonbridged analogue [Re(η–C_5H_5)$_2$Cl] **(I)**. Geometry optimisations on **I** and **II** resulted in bond lengths, interatomic distances and angles given in **Table 4.9**. The calculations gave a structure with C_{2v} symmetry for **I** but the lowest energy geometry found for **II** had an angle of θ = 175.6° between the Re-Cl bond and the Re…C(11) vector. This is somewhat larger than that found experimentally for the compound **39** but was consistently reproduced from a number of different starting geometries. Frequency calculations on the optimised structures gave only positive frequencies for **I** but for **II** an imaginary frequency of 40i cm^{-1} was found corresponding to a wagging of the Cl atom in the xz plane. The structure was re-optimised including the gradient corrections in the SCF convergence. Studies on a number of transition metal carbonyl complexes have shown this procedure to give longer distances in closer agreement with experiment.[39] In this case distances (also given in **Table 4.9**) were found to be longer but in less good agreement with experimental observations and a C(11)…Re-Cl angle of θ = 165.5° was the result. A frequency calculation on this structure gave all real frequencies confirming that a local minimum had been identified. The Cl wag was the lowest energy vibration with a wave number of 40 cm^{-1}. It is evident that the Cl wag in the xz plane (defined in **Figure 4.13**) is a very low energy vibration.

	II (calc)[a]	**II** (calc)[b]	**39**	**I** (calc)	**I** (exp)[35]
Re-Cl	2.479	2.433	2.4383(13)	2.461	2.438(3)
Re-C(1)	2.234	2.208	2.175(5)	2.217	2.210(20)
Re-C(2)	2.302	2.243	2.218(5)	2.217	2.220(10)
Re-C(3)	2.340	2.290	2.245(5)	2.292	2.286(9)
Re-C(4)	2.343	2.287	2.245(5)	2.292	2.280(10)
Re-C(5)	2.250	2.225	2.199(5)	2.302	2.230(10)
Re-C(11)	2.885	2.864	2.8912		
Re-Cp_{cent} (ave)	1.939	1.893	1.855	1.912	1.886
C(1)-C(2)	1.456	1.446	1.454(7)	1.436	1.400(20)
C(2)-C(3)	1.420	1.412	1.398(8)	1.427	1.410(20)
C(3)-C(4)	1.450	1.443	1.439(9)	1.420	1.440(20)
C(4)-C(5)	1.429	1.415	1.416(8)	1.420	1.380(20)
C(1)-C(5)	1.460	1.447	1.448(7)	1.427	1.400(20)
θ	165.6	175.4	170.44	180.0[c]	179.4[c]
α	57.0	55.2	53.1	36.5	40.2
β	123.0	124.8	126.9	143.5	139.8
ϕ	21.8	22.0	20.9, 22.0		
ε	99.9	99.2	95.8		
γ	130.0	130.0	131.3	149.6	147.6

[a] Non-local correction included throughout the calculation
[b] Non-local correction not used in calculating gradients
[c] For **VII** θ defined as X....Re-Cl where X is the centroid of the four η-cyclopentadienyl carbon atoms furthest from Cl.

Table 4.9 Calculated bond lengths (Å) and angles (°) for $[Re\{(\eta\text{-}C_5H_4)CH_2(\eta\text{-}C_5H_4)\}Cl]$ **(II)** and $[Re(\eta\text{-}C_5H_5)_2Cl]$ **(I)**

For comparative purposes the geometry of **II** was also optimised with C_{2v} symmetry. Molecular orbital (MO) schemes for **I** and **II**, with C_{2v} symmetry, are given in **Figure 4.15** together with the orbital energy levels for the corresponding fragments, $[Re\{(\eta\text{-}C_5H_4)CH_2(\eta\text{-}C_5H_4)\}]$ and $[Re(\eta\text{-}C_5H_5)_2]$, also with C_{2v} symmetry. The fragment

calculations were performed on the same geometry as that found in the optimised molecular structures. There are marked differences in the two molecular energy schemes, notably the b_1 HOMO is of higher energy in **II** than **I**, whereas the a_1 HOMO-1 is significantly more stable in **II** than **I**. Representations of these orbitals are shown in **Figure 4.16(a)** and **4.16(c)**.

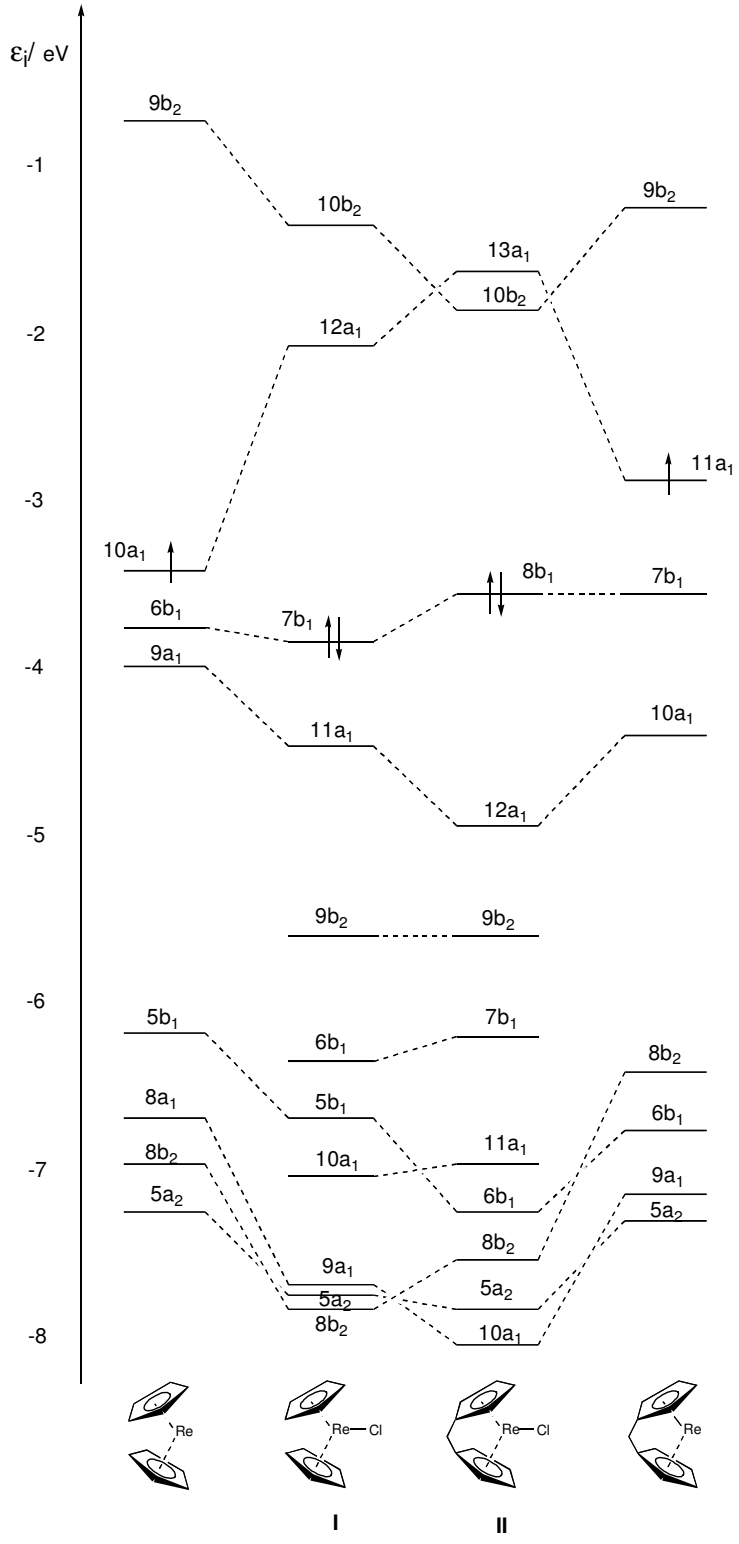

Figure 4.15 MO schemes for the fragment $[Re(\eta{-}C_5H_5)_2]$, $[Re(\eta{-}C_5H_5)_2Cl]$ **(I)**, $[Re\{(\eta{-}C_5H_4)CH_2(\eta{-}C_5H_4)\}Cl]$ **(II)**, and the fragment $[Re\{(\eta{-}C_5H_4)CH_2(\eta{-}C_5H_4)\}]$. Dashed lines correlate related orbitals. The levels in the schemes for **I** and **II** which are not correlated with fragment orbitals are principally Cl 3p in origin

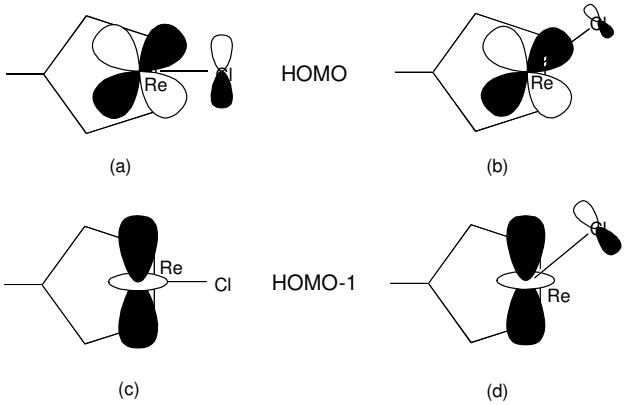

Figure 4.16 Representations of selected orbitals. HOMO of **II** when (a) $\theta = 180°$ (b) $\theta < 180°$. HOMO-1 of **II** when (c) $\theta = 180°$ (d) $\theta < 180°$

The relative energies of the HOMO and HOMO-1, and other energy differences in the metal cyclopentadienyl bonding orbitals, may be traced back to energy differences between the two parent fragments. The larger inter-ring angle α in the *ansa*-bridged analogue leads to a greater energy spread of the three frontier metal orbitals (**Section 1.1.2**). In the fragments, in addition to the differences in the lower a_1 and b_1 orbitals already noted, an upper a_1 orbital ($11a_1$) is significantly raised in energy in the fragment [Re{(η–C_5H_4)CH_2(η–C_5H_4)}] compared with the analogous orbital ($10a_1$) in the fragment [Re(η–C_5H_5)$_2$]. This a_1 orbital, shown in **Figure 4.17**, is the one available to bind a group in the central position. Thus it may be anticipated that it will be less effective in covalent bonding when the rings are linked by an *ansa*-bridge. Population analysis shows that in **II** the $11a_1$ fragment orbital has an occupation of 0.37 electrons and the Cl $3p_z$ orbital 1.61 electrons, whereas in **I** the corresponding fragment 10 a_1 orbital has an occupancy of 0.46 electrons and the Cl $3p_z$ orbital 1.55 electrons. Thus it can be concluded that bonding in the central position is less favoured by the introduction of an *ansa*-bridge. This result is consistent with the theoretical predictions for the trihydrides described in **Section 4.2.7** where the central H_A is shown to bind less effectively than the lateral H_B upon introduction of an *ansa*-bridge.

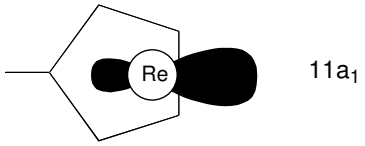

Figure 4.17 Representation of the $11a_1$ orbital of the fragment [Re{(η–C_5H_4)CH_2(η–C_5H_4)}]

Geometry optimisation of the analogous *ansa*-bridged hydride [Re{(η–C_5H_4)CH_2(η–C_5H_4)}H] gave a structure with C_{2v} symmetry and a C(11)...Re-H angle of 180°, which suggests that the pπ electrons of the Cl atom might well be responsible for the distortion.

Further analysis was undertaken with a linear transit calculation on **II** in which the C(11)...Re-Cl angle, θ, was varied between 140° and 180° and the remainder of the molecule was geometry optimised. The energy variations with angle obtained for the molecule and the upper orbitals are shown in **Figure 4.18**. This confirms the presence of a very shallow minimum in the energy surface at a C(11)…Re-Cl angle θ *ca.* 175°, and shows that as θ decreases, the energy of the HOMO drops and the HOMO-1 rises. The reason for these changes is evident from the nodal properties of these two orbitals shown in **Figure 4.16**. The HOMO, whilst largely metal in character, is metal Cl pπ antibonding (**Figure 4.16(a)**). Moving the Cl atom off the central position relieves the anti-bonding interaction (**Figure 4.16(b)**). The HOMO-1 is by contrast metal Cl non-bonding when the Cl atom is centrally placed (**Figure 4.16(c)**), but becomes anti-bonding as the Cl is moved to one side (**Figure 4.16(d)**). It appears to be this π interaction which favours a small displacement of the Cl atom. That it does not also occur in the nonbridged compound is due to the fact that the σ-bonding of the halide is more directed in this case.

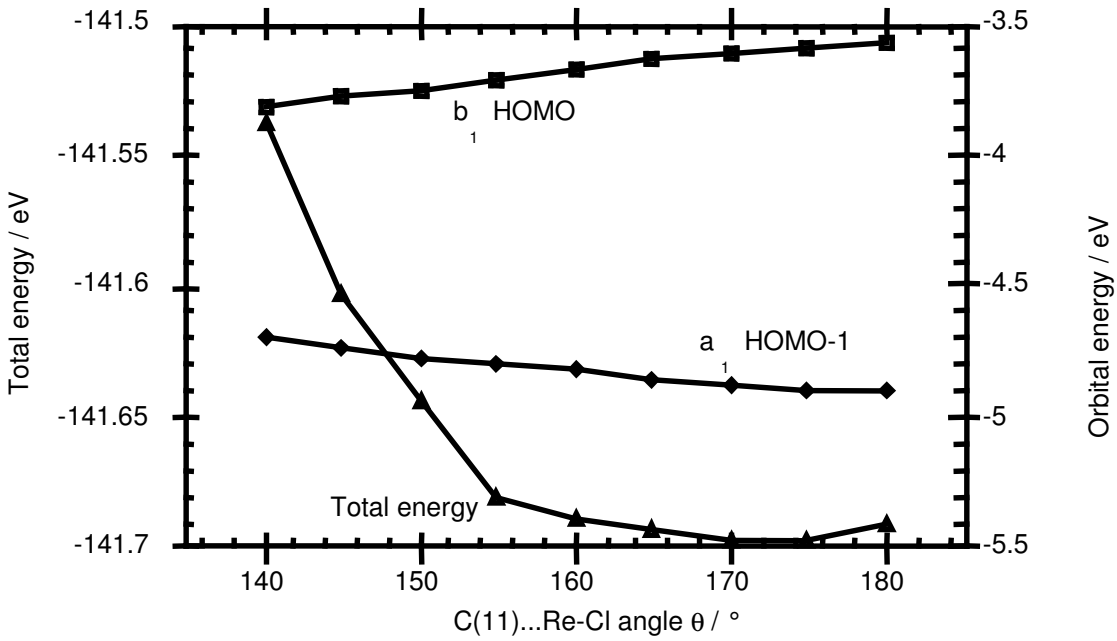

Figure 4.18 Plot of the variation of the total energy, the energy of the HOMO and the HOMO-1 of [Re{(η–C_5H_4)CH_2(η–C_5H_4)}Cl] **II**, with C(11)…Re-Cl angle, θ

4.5 Summary

This chapter has described the synthesis and characterisation of new cyclohexyl-bridged *ansa*-metallocenes of tungsten. The corresponding trihydride complex, $[W\{(\eta-C_5H_4)C(C_5H_{10})(\eta-C_5H_4)\}H_3][BF_4]$ displays a large temperature dependent H-H coupling constant with J_{AB} varying from 17500 Hz at 223 K to 2900 Hz at 147 K. Theoretical studies have shown that as the inter-ring angle α is increased and the bending angle β decreased by the introduction of a sterically constraining *ansa*-bridge, the central H atom binds less effectively to the metal and the rings become more tightly bound. The reduced bonding interaction between the central hydride and the metal facilitates exchange between central and lateral hydrogens and the onset of quantum mechanical exchange coupling. Spectroscopic evidence also indicates that the presence of a silicon- or ethylene-bridge in $[Nb\{(\eta-C_5H_4)SiMe_2(\eta-C_5H_4)\}H_3]$ and $[Nb\{(\eta-C_5H_4)C_2Me_4(\eta-C_5H_4)\}H_3]$ increases the magnitude of the quantum mechanical exchange coupling contribution to J_{AB} relative to the analogous nonbridged compound.

The first carbon-bridged *ansa*-rhenocene complex $[Re\{(\eta-C_5H_4)CMe_2(\eta-C_5H_4)\}Cl]$ has been prepared and is shown crystallographically to be unsymmetrical with the angle defined by the Re-bridgehead carbon vector and the chlorine atom found to be 170.4°.[40] Density functional studies support the observation of an unsymmetrical molecular structure, with the presence of the *ansa*-bridge responsible for displacement of the chlorine atom from the central position.

The new chemistry described in Chapter 4 is presented in **Scheme 4.7**.

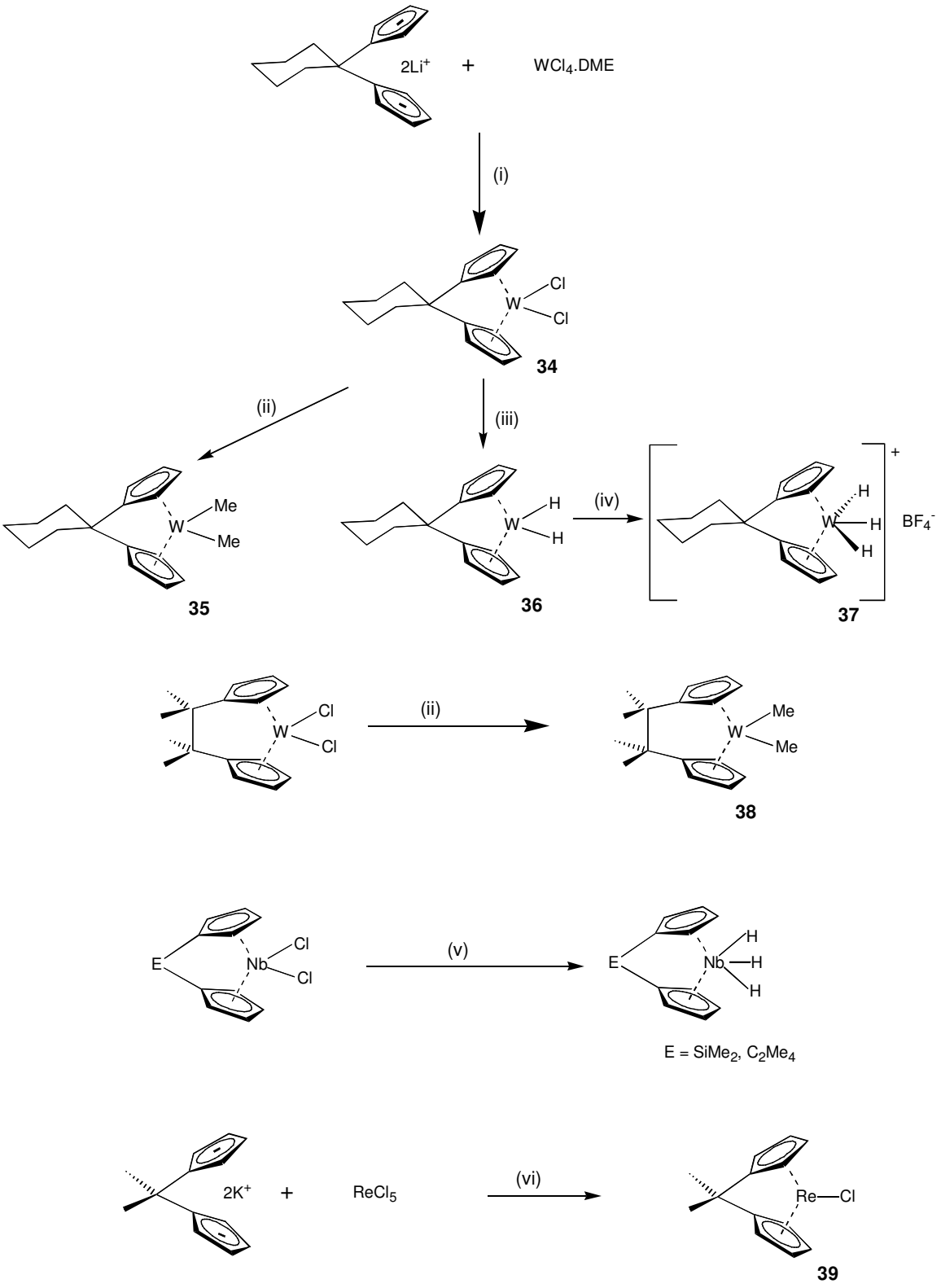

Conditions: (i) Diethyl ether, 3 days. (ii) $ZnMe_2$ in toluene.
(iii) $LiBEt_3H$ in THF. (iv) HBF_4 in diethyl ether.
(v) $[Na\{AlH_2(OCH_2CH_2OCH_3)_2\}]$ in toluene. (vi) DME.

Scheme 4.7 New chemistry presented in Chapter 4

4.6 References

1 M. L. H. Green, J. A. McCleverty, L. Pratt and G. Wilkinson, *J. Chem. Soc.*, 1961, 4854.

2 S. L. J. Conway, T. Dijkstra, L. H. Doerrer, J. C. Green, M. L. H. Green and A. H. H. Stephens, *J. Chem. Soc., Dalton Trans.*, 1998, 2689.

3 A. Chernega, J. Cook, M. L. H. Green, L. Labella, S. J. Simpson, J. Souter and A. H. H. Stephens, *J. Chem. Soc., Dalton Trans.*, 1997, 3225.

4 (a) S. Sabo-Etienne and B. Chaudret, *Chem. Rev.*, 1998, **98**, 2077. (b) F. Maseras, A. Lledos, E. Clot and O. Eisenstein, *Chem. Rev*. 2000, **100**, 601.

5 A. Antiñolo, B. Chaudret, G. Commenges, M. Fajardo, F. Jalon, R. H. Morris, A. Otero and C. T. Schweltzer, *J. Chem. Soc., Chem. Commun.*, 1988, 1210.

6 M. D. Curtis, L. G. Bell and W. M. Butler, *Organometallics*, 1985, **4**, 701.

7 D. M. Heinekey, *J. Am. Chem. Soc.*, 1991, **113**, 6074.

8 J. F. LeBoeuf, O. Lavastre, J. C. Leblanc and C. Moise, *J. Organomet. Chem.*, 1986, **418**, 359.

9 S. Sabo-Etienne, B. Chaudret, H. A. El-Makarim, J. C. Barthelat, J. P. Daudley, S. Ulrich, H. H. Limbach and C. Moise, *J. Am. Chem. Soc.*, 1995, **117**, 11602.

10 F. A. Jalon, A. Otero, B. Manzano, E. Villasenor and B. Chaudret, *J. Am. Chem. Soc.*, 1995, **117**, 10123.

11 D. M. Heinekey, N. G. Payne and G. K. Schulte, *J. Am. Chem. Soc.*, 1988, **110**, 2303.

12 K. W. Zlim, D. M. Heinekey, J. M. Millar, N. G. Payne, S. P. Neshyba, J. C. Duchamp and J. Szczyrba, *J. Am. Chem. Soc.*, 1990, **112**, 920.

13 D. M. Heinekey, A. S. Hinkle and J. D. Close, *J. Am. Chem. Soc.*, 1996, **118**, 5353.

14 R. B. Girling, P. Grebenik and R. N. Perutz, *Inorg. Chem.*, 1986, **25**, 31.

15 G. Parkin and J. E. Bercaw, *J. Chem. Soc., Chem. Commun.*, 1989, 255.

16 P. Grebenik, Part II Thesis, University of Oxford, 1974.

17 *gNMR simulation package, V3.6 for Windows*, 1995, Cherwell Scientific, Oxford.

18 A. Antiñolo, F. Carrillo-Hermosilla, B. Chaudret, M. Fajardo, J. Fernadez-Baeza, M. Lanfranchi, H.H. Limbach, M. Maurer, A. Otero and M. A. Pellinghelli, *Inorg. Chem.*, 1996, **35**, 7873.

19 R. H. Crabtree, P. E. Siegbahn, O. Eisenstein, A. Rheingold and T. F. Koetzle, *Acc. Chem. Res.*, 1996, **29**, 348 and references therein.

20 B. P. Patel, J. Wessel, W. Yao, J. J. C. Lee, E. Peris, T. F. Koetzle, G. P. A. Yap, J. B. Fortin, J. S. Ricci, G. Sini, A. Albinati, O. Eisenstein, A. Rheingold and R. H. Crabtree, *N. J. Chem.*, 1997, **21**, 413.

21 J. A. Ayllon, S. Sabo-Etienne, B. Chaudret, S. Ulrich and H. H. Limbach, *Inorg. Chim. Acta*, 1997, **259**, 1.

22 J. C. Green, , 2000, Personal communication.

23 C. C. Wilson, N. Shankland and A. J. Florence, *J. Chem. Soc., Faraday Trans.*, 1996, **92**, 5051.

24 C. C. Wilson, N. Shankland and A. J. Florence, *Chem. Phys. Lett.*, 1996, **253**, 103.

25 S. L. J. Conway, Part II Thesis, University of Oxford, 1997.

26 J. C. Green and A. Scottow, *N. J. Chem.*, 1999, **23**, 651.

27 J. C. Green, *Chem. Soc. Rev.*, 1998, 263.

28 N. J. Bailey, "*ansa*-Bridged Metallocene Chemistry of Niobium.", D. Phil. Thesis, University of Oxford, 1998.

29 J. A. Labinger and K. S. Wong, *J. Organomet. Chem.*, 1979, **170**, 373.

30 R. A. Bell, S. A. Cohen, N. M. Doherty, R. S. Threlkel and J. E. Bercaw, *Organometallics*, 1986, **5**, 972.
31 J. H. Shin and G. Parkin, *J. Chem. Soc., Chem. Commun.*, 1999, 887.
32 D. M. Heinekey and G. L. Gould, *J. Am. Chem. Soc.*, 1989, **111**, 5502.
33 D. M. Heinekey and G. L. Gould, *Organometallics*, 1991, **10**, 2977.
34 D. M. Heinekey and C. E. Radzewich, *Organometallics*, 1999, **18**, 3070.
35 C. Apostolidos, B. Kanellakopulos, R. Maier, J. Rebizant and M. L. Ziegler, *J. Organomet. Chem*, 1991, **409**, 243.
36 J. C. Green and C. N. Jardine, *J. Chem. Soc., Dalton Trans.*, 1998, 1057.
37 S. Barlow, M. J. Drewitt, T. Dijkstra, J. C. Green, D. O'Hare, C. Wittingham, H. H. Wynn, D. P. Gates, I. Manners and J. K. Pudelski, *Organometallics*, 1998, **17**, 2113.
38 J. C. Green and C. N. Jardine, *J. Chem. Soc. Dalton Trans.*, 1998, 1057.
39 L. Fan and T. Ziegler, *J. Chem. Phys.*, 1991, **95**, 7401.
40 S. L. J. Conway, L. H. Doerrer, J. C. Green, M. L. H. Green, A. Scottow and A. H. H. Stephens, *J. Chem. Soc., Dalton Trans.,* 2000, 329.